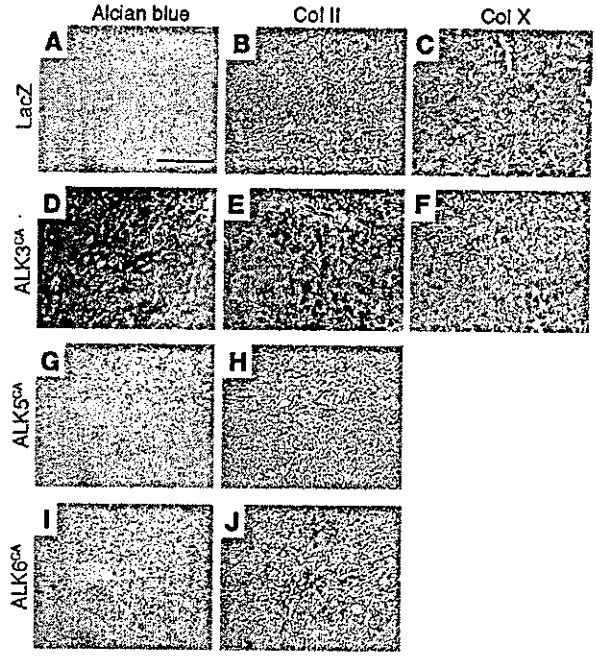

Figure 3
ALK3^{CA} gene transduction increases Alcian blue–positive matrix and type II collagen deposition in pellet cultures of SFs. (**A–J**) Adenovirus-infected SF pellets were fixed with 3.7% formaldehyde after 3 weeks of culture and then were subjected to Alcian blue staining (**A**, **D**, **G**, and **I**) or immunostaining with anti–type II collagen (**B**, **E**, **H**, and **J**) or anti–type X collagen (Col X) (**C** and **F**). Distinct Alcian blue (**D**) and type II collagen (**E**) staining was observed in ALK3^{CA}-expressing cultures. ALK6^{CA}-expressing cultures showed weaker staining (**I** and **J**), and no positive staining was observed in ALK5^{CA} virus–infected (**G** and **H**) or LacZ virus–infected (**A** and **B**) cultures. No type X collagen immunostaining was observed in cultures expressing LacZ or ALK3^{CA} (**C** and **F**). Scale bar: 100 μm.

overexpression was able to target cartilage formation without subsequent bone formation in vivo.

Segregation of ALK signaling pathways. ALK signaling is known to be mediated by both the Smad pathways and MAP kinase pathways, especially the p38 pathways (31–33). We therefore attempted to distinguish the roles of the Smad pathways and p38 pathways from each other using a specific p38 inhibitor or adenovirus vectors. Smad6 coexpression or treatment of the cultures with the p38 inhibitor SB203580 completely abrogated the chondrogenic gene expression induced by ALK3^{CA} (Figure 2, B and C). These results indicate that both the Smad pathways and the p38 MAP kinase pathways are required for the differentiation. Although Smad1 expression alone (MOI = 20) or a small amount of ALK^{CA} virus (MOI = 2) failed to induce type II collagen expression in SFs, both had synergistic effects, and robust upregulation of type II collagen gene was observed by coinfection of Smad1 virus (MOI = 20) and ALK3^{CA} virus (MOI = 2) (Figure 5A). Interestingly, activation of p38 pathways alone by MKK6^{CA} expression in SFs induced rapid induction of Sox9 and type II collagen, which declined rapidly, however, and type X collagen expression was subsequently increased (Figure 5B). Coexpression of Smad1 together with MKK6^{CA} not only reduced type X collagen expression but also maintained type II collagen expression in the cells (Figure 5B). Pellet cultures infected

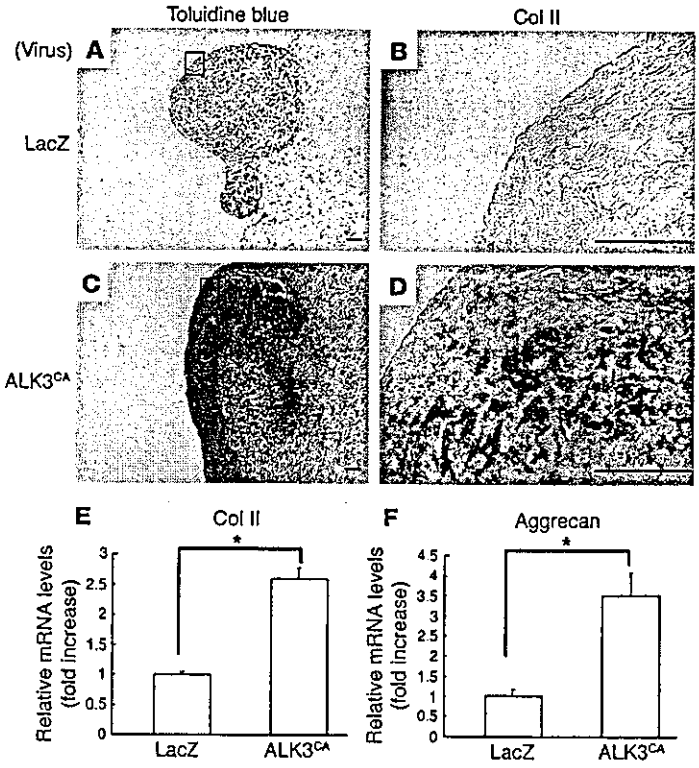

Figure 4
ALK3^{CA}-transduced SFs form cartilage matrix in vivo. (**A–D**) Three weeks after transplantation into nude mice, pellets were recovered and stained with toluidine blue (**A** and **C**) and immunostained with anti–type II collagen (**B** and **D**). Type II collagen immunohistochemistry was shown in the enlarged features of the rectangular area in the toluidine blue staining. Distinct positive staining was observed in ALK3^{CA}-expressing cultures (**B** and **D**) in contrast to LacZ virus–infected cultures (**A** and **C**). Scale bars: 100 μm. (**E** and **F**) Real-time PCR analysis of type II collagen and aggrecan. Their expression was significantly higher in ALK3^{CA}-expressing pellets than in LacZ-expressing pellets. *$P < 0.001$ (significantly different).

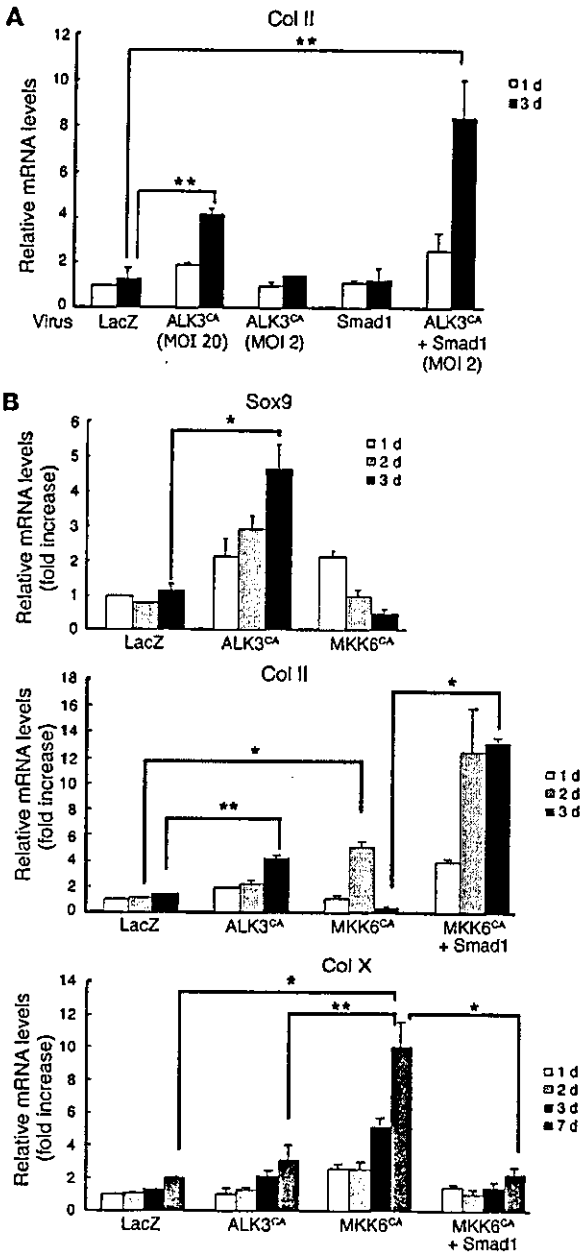

Figure 5
Segregation of downstream signaling pathways of ALK3. (A) Synergistic effect of Smad1 expression on the chondrogenic effects of the ALK3^{CA} virus. Expression of Smad1 (MOI = 20) together with ALK3^{CA} virus (MOI = 2) strongly induced expression of type II collagen in SFs. White bars indicate type II collagen expression on day 1 of cultures, and black bars indicate that on day 3. $^{**}P < 0.005$ (significantly different). (B) MKK6-p38 pathways promote terminal chondrocytic differentiation of SFs. Mandatory activation of p38 pathways by expression of MKK6^{CA} using adenovirus vectors rapidly activated expression of the Sox9 and type II collagen genes, which rapidly declined, while expression of a terminal chondrocytic differentiation marker, type X collagen, was gradually increased. Adenovirus vector–mediated overexpression of Smad1 together with MKK6^{CA} suppressed type X collagen expression and maintained type II collagen expression in SFs. $^{*}P < 0.001$; $^{**}P < 0.005$ (significantly different).

with MKK6^{CA} virus were positively stained by type X collagen immunostaining as well as Alizarin red staining, which was suppressed by Smad1 virus coinfection (Figure 6).

Type X collagen expression and p38 activation in synovial cells in osteoarthritic joints. To examine the role of p38 activation in the development of degenerative changes in the articular cartilage, we next analyzed synovial tissues in the mouse model of osteoarthritis. After ACL and MM resection, the animals developed degenerative joint changes mimicking osteoarthritis. Osteochondrophytes were formed at the posterior edge of the femoral condyle and they were positively stained by anti-type X collagen as well as toluidine blue (rectangular areas in Figure 7, A and C) 4 weeks after the operation (corresponding to the stage of moderate osteoarthritis). Clusters of migrating synovial cells were observed adjacent to the osteochondrophytes (Figure 7B, arrowheads), where future osteochondrophytes will develop, and they were weakly stained by toluidine blue and anti-type X collagen at the marginal area between synovium and osteophytes (rectangular areas in Figure 7, B and D). This region was also positively stained by anti-phospho-p38 (Figure 7F). No positive staining was observed in the normal synovium, however (data not shown).

Discussion

The signaling events leading to chondrogenesis still remain elusive, although there is accumulating evidence that TGF-β superfamily cytokines may play an important role (19–22). The receptors of TGF-β family members are composed of two different types of serine/threonine kinase receptors, known as type I and type II (31, 34, 35). Type II receptors are constitutively active kinases and phosphorylate type I receptors, also called ALKs. Type I receptors in turn mediate specific intracellular signaling pathways and therefore determine the specificity of the downstream signaling. So far, seven type I receptors have been identified, ALKs 1–7. ALK3 (BMPR-IA) and ALK6 (BMPR-IB) are structurally similar to each other and function as BMP receptors, while ALK5 and ALK4 work as type I TGF-β receptors. Using the adenovirus vector system, Fujii et al. reported that ALK1^{CA}, ALK2^{CA}, ALK3^{CA}, and ALK6^{CA} induced osteoblastic differentiation of C2C12 myoblasts and that ALK3^{CA} or ALK6^{CA} introduction induced chondrocytic differentiation of ATDC teratocarcinoma cells (27).

In the present study, we focused on the regulation of chondrogenic differentiation of primary SFs obtained from rheumatoid arthritis patients. SFs have chondrogenic potential (15, 16) and can migrate into articular cartilage defects, where they deposit a scar-like tissue as Hunziker et al. pointed out (14), suggesting that SFs have anabolic effects on joint homeostasis and are involved in the restoration process of articular cartilage. We demonstrated that adenovirus vector–mediated ALK3^{CA} gene expression induced robust induction of chondrocyte-specific gene expression in SFs in a ligand-independent manner. Clear induction of Sox9, a key transcription factor regulating chondrogenesis (36, 37), followed by type II collagen and aggrecan expression, was observed in the ALK3^{CA}-expressing cultures, while type X collagen was only weakly induced in the cultures and no osteocalcin expression could be found (Figures 2 and 5). Induction of these chondrocyte-specific genes through ALK3^{CA} expression was not observed in skin fibroblasts, suggesting the cell specificity of the events (data not

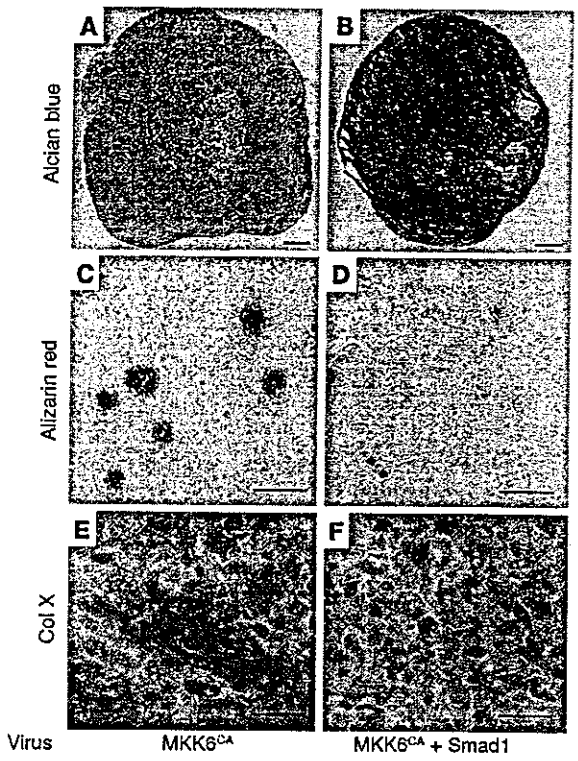

Figure 6
Induction of Alizarin red staining and type X collagen in MKK6-transduced SFs in pellet cultures. (**A**–**F**) SFs infected with MKK6^{CA} virus alone (**A**, **C**, and **E**) or together with Smad1 virus (**B**, **D**, and **F**) were subjected to pellet culture. Cultures were fixed with 3.7% formaldehyde 3 weeks later, and then stained with Alcian blue (**A** and **B**), Alizarin red (**C** and **D**) or anti–type X collagen (**E** and **F**). Note the increased Alcian blue staining and the reduced Alizarin red activity and type X collagen immunoactivity with Smad1 coexpression. Scale bars:100 μm (**A**–**D**) and 50 μm (**E** and **F**).

shown). The chondrogenic effect of ALK3^{CA} virus was further confirmed histologically by pellet cultures performed in vitro and in vivo (Figures 3 and 4). Induction of neither the osteoblast markers osteopontin and osteocalcin nor the terminal chondrocyte differentiation markers type X collagen and mineralization was observed in ALK3^{CA}-expressing cells (Figures 2, 3, 5, and 6). These results suggest that ALK3 signaling, that is, BMP signaling, has both stimulatory and regulatory roles in chondrogenesis: to induce the chondrogenic differentiation of SFs and at the same time to block their osteoblastic or hypertrophic differentiation. Despite the structural similarity between ALK3 and ALK6, the ALK6^{CA} virus was much less efficient in chondrogenesis, the reason for which remains to be clarified. Although many studies have demonstrated a prochondrogenic effect for TGF-β (15, 16, 20–22), we failed to find an anabolic effect for ALK5^{CA} which is expected to mimic TGF-β signaling, on the chondrogenic differentiation of SFs. We cannot fully explain the discrepancy between our results and those of previous studies, but Robbins and coworkers recently reported that adenovirus vector–mediated TGF-β gene transduction into arthritic joints in fact exacerbated cartilage degradation (38), raising the possibility that sustained activation of TGF-β signaling, via ALK5, has instead a negative effect on chondrogenesis. Further study will be required to elucidate the difference between TGF-β and BMP signaling.

The signaling of TGF-β/BMPs is transduced by Smad family members (31, 34, 35). Receptor-regulated Smads (R-Smads) are direct substrates of type I receptors and are phosphorylated at the C-terminal SSV/MS motif. R-Smads then form heteromeric complexes with common-mediator Smads and translocate into the nuclei, where they regulate transcription of target genes. In addition to Smad pathways, there is evidence that MAP kinase cascades are also implicated in ALK signaling, in which TGF-β–activating kinase (TAK1), a member of the MAP kinase kinase kinase family, plays a key role. TAK1 activates MAP kinase kinase in combination with an adaptor molecule, TAB1, which leads to JNK and p38 activation (32). The role of p38 in chondrogenesis has recently attracted particular interest because p38 inhibitors such as SB203580 suppress the chondrogenic differentiation of ATDC5 cells induced by growth/differentiation factor-5 (33, 39). However, the exact roles of the Smad pathways and p38 pathways in chondrocyte differentiation are not yet fully clarified. We used a combination of adenoviral gene delivery and a chemical inhibitor to segregate the roles of these two pathways downstream of ALK3 activation and found that (a) inhibitory Smad (Smad6) expression or treatment with the p38 inhibitor SB203580 suppressed the effect of ALK3^{CA} expression (Figure 2) (b) Smad1 synergistically augmented the effect of ALK3^{CA} (Figure 5A), and (c) activation of p38 pathways alone by MKK6^{CA} expression induced the hypertrophic differentiation markers type X collagen and mineralization in SFs, which was suppressed by Smad1 coexpression (Figures 5B and 6). These results suggest that although both Smad and p38 activation is necessary for chondrogenic differentiation of SFs, sustained activation of p38 pathways alone prompts the terminal differentiation of the cells. Consistent with our results, Zhen et al. (40) reported that parathyroid hormone inhibits type X collagen expression in hypertrophic chondrocytes by suppressing p38 pathways. Von der Mark et al. (41) reported the focal appearance of type X collagen in osteoarthritic cartilage, which may be involved in the degenerative changes of the articular cartilage and in the pathogenesis of osteoarthritis. Using the mouse model of osteoarthritis, we found that activated p38 is associated with type X colla-

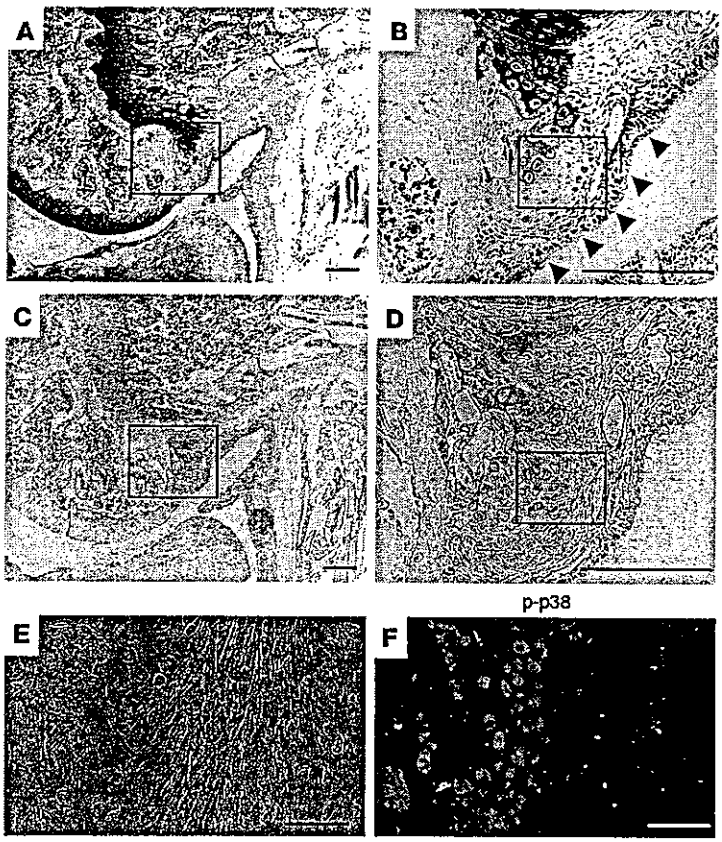

Figure 7
Histological analysis of knee joints in the mouse ACL and MM resection model. (**A–F**) Toluidine blue staining (**A** and **B**) and type X collagen immunostaining (**C** and **D**) at the marginal area between the articular cartilage and synovium. **B** and **D** present higher-magnification views of **A** and **C**, respectively. Osteochondrophytes were formed at the posterior edge of the femoral condyle, and they were positively stained by anti–type X collagen as well as toluidine blue (rectangular areas in **A** and **C**). Clusters of migrating synovial cells were observed adjacent to the osteochondrophytes (**B**, arrowheads) where future osteochondrophytes will develop, and they were positively stained by anti–type X collagen at the marginal area between synovium and osteophytes (rectangular area in **D**). This region was also positively stained by anti–phospho-p38 (**F**). **E** and **F** represent phase-contrast microscopy (**E**) and immunostaining with anti–phospho-p38 (**F**) of the rectangular area in **D**. Positive phospho-p38 staining was observed at the area of osteochondrophytes as well as the marginal synovium. Scale bars: 500 μm (**A–D**) and 50 μm (**E** and **F**).

gen expression in the synovial tissues adjacent to osteochondrophytes as well as in the degenerative cartilage (Figure 7).

Smad pathways not only are required for chondrogenic differentiation of SFs but also critically regulate the stage of differentiation of the cells and suppress their terminal differentiation process. Consistent with our findings, Scharstuhl recently reported inhibitory action of Smad7 in TGF-β–induced chondrocyte proliferation and proteoglycan production (42), indicating a critical role for Smad pathways. Hidaka and coworkers (43) demonstrated that adenovirus vector–mediated BMP-7 expression in chondrocytes accelerates the cartilage repair process. More recently, Lories and colleagues (44) demonstrated that BMP-2 and BMP-6 expressed in arthritic synovium are regulated by proinflammatory cytokines and differentially modulate fibroblast-like synoviocyte apoptosis, and Fukui et al. (45) found that BMP-2 expression was increased by proinflammatory cytokines in normal and osteoarthritis chondrocytes. These findings, combined with our observations, suggest that although BMPs have favorable effects on the repair process of articular cartilage, they may have proapoptotic and/or degenerative effects on the cells when p38 pathways are overactivated. Our findings suggest an important role for p38 signal transduction pathways in chondrocytes and SFs, leading to degenerative joint disorders, and suggest the potential utility of p38 modifiers in the treatment of rheumatoid arthritis and/or osteoarthritis. In fact, p38 kinase modifiers are now in clinical trials to treat rheumatoid arthritis (46). Based on our observations, we would like to propose that SFs are an excellent source for chondroprogenitors, which can be differentiated into chondrocytes via ALK3 activation, and that activation of the Smad pathway while controlling the degree of p38 activation may be a way to generate committed chondrocytes for the repair and/or replacement of cartilage.

Acknowledgments

The authors thank R. Yamaguchi and M. Ikeuchi (Department of Orthopaedic Surgery, The University of Tokyo), who provided expert technical assistance; K.L. Insogna (Yale University) for critical reading of the manuscript; and Y. Iwamoto (Thomas Jefferson University) for type II collagen and aggrecan probes. ALK and Smad adenovirus vectors were kindly provided by K. Miyazono (The University of Tokyo) and T. Imamura (The Cancer Institute of the Japanese Foundation for Cancer Research). This work was in part supported by Grants-in-Aid from the Ministry of Education, Culture, Sports, Science and Technology of Japan, Health Science research grants from the Ministry of Health and Welfare of Japan and an Uehara Memorial Award to S. Tanaka.

Received for publication August 28, 2003, and accepted in revised form January 6, 2004.

Address correspondence to: Sakae Tanaka, Department of Orthopaedic Surgery, Faculty of Medicine, The University of Tokyo, 7-3-1 Hongo, Bunkyo-ku, Tokyo 113-0033, Japan. Phone: 81-3-3815-5411 ext. 33376; Fax: 81-3-3818-4082; E-mail: TANAKAS-ORT@h.u-tokyo.ac.jp.

1. Hunziker, E.B. 2002. Articular cartilage repair: basic science and clinical progress. A review of the current status and prospects. *Osteoarthritis Cartilage.* 10:432–463.
2. Poole, A.R., et al. 2001. Composition and structure of articular cartilage: a template for tissue repair. *Clin. Orthop.* 391:S26–S33.
3. Poole, A.R. 2003. What type of cartilage repair are we attempting to attain? *J. Bone Joint Surg. Am.* 85-A(Suppl. 2):40–44.
4. Hunziker, E.B. 2003. Tissue engineering of bone and cartilage. From the preclinical model to the patient. *Novartis Found. Symp.* 249:70–85, 170–174, and 239–141.
5. Bruder, S.P., et al. 1998. Mesenchymal stem cells in osteobiology and applied bone regeneration. *Clin. Orthop.* 355:S247–S256.
6. Matsusue, Y., Yamamuro, T., and Hama, H. 1993. Arthroscopic multiple osteochondral transplantation to the chondral defect in the knee associated with anterior cruciate ligament disruption. *Arthroscopy.* 9:318–321.
7. Bentley, G., et al. 2003. A prospective, randomised comparison of autologous chondrocyte implantation versus mosaicplasty for osteochondral defects in the knee. *J. Bone Joint Surg. Br.* 85:223–230.
8. Peterson, L., Minas, T., Brittberg, M., and Lindahl, A. 2003. Treatment of osteochondritis dissecans of the knee with autologous chondrocyte transplantation: results at two to ten years. *J. Bone. Joint Surg. Am.* 85-A(Suppl 2):17–24.
9. Peterson, L., Brittberg, M., Kiviranta, I., Akerlund, E.L., and Lindahl, A. 2002. Autologous chondrocyte transplantation. Biomechanics and long-term durability. *Am. J. Sports Med.* 30:2–12.
10. Minas, T., and Nehrer, S. 1997. Current concepts in the treatment of articular cartilage defects. *Orthopedics.* 20:525–538.
11. Hangody, L., Feczko, P., Bartha, L., Bodo, G., and Kish, G. 2001. Mosaicplasty for the treatment of articular defects of the knee and ankle. *Clin. Orthop.* 391:S328–S336.
12. Firestein, G.S. 2003. Evolving concepts of rheumatoid arthritis. *Nature.* 423:356–361.
13. Takayanagi, H., et al. 1999. Suppression of arthritic bone destruction by adenovirus-mediated csk gene transfer to synoviocytes and osteoclasts. *J. Clin. Invest.* 104:137–146.
14. Hunziker, E.B., and Rosenberg, L.C. 1996. Repair of partial-thickness defects in articular cartilage: cell recruitment from the synovial membrane. *J. Bone Joint Surg. Am.* 78:721–733.
15. Nishimura, K., et al. 1999. Chondroprogenitor cells of synovial tissue. *Arthritis Rheum.* 42:2631–2637.
16. De Bari, C., Dell'Accio, F., Tylzanowski, P., and Luyten, F.P. 2001. Multipotent mesenchymal stem cells from adult human synovial membrane. *Arthritis Rheum.* 44:1928–1942.
17. De Bari, C., et al. 2003. Skeletal muscle repair by adult human mesenchymal stem cells from synovial membrane. *J. Cell Biol.* 160:909–918.
18. O'Connell, J.X. 2000. Pathology of the synovium. *Am. J. Clin. Pathol.* 114:773–784.
19. Wozney, J.M. 1989. Bone morphogenetic proteins. *Prog. Growth Factor Res.* 1:267–280.
20. Kulyk, W.M., Rodgers, B.J., Greer, K., and Kosher, R.A. 1989. Promotion of embryonic chick limb cartilage differentiation by transforming growth factor-beta. *Dev. Biol.* 135:424–430.
21. Lafeber, F.P., Vander Kraan, P.M., Van Roy, J.L., Huber-Bruning, O., and Bijlsma, J.W. 1993. Articular cartilage explant culture; an appropriate in vitro system to compare osteoarthritic and normal human cartilage. *Connect. Tissue Res.* 29:287–299.
22. Denker, A.E., Nicoll, S.B., and Tuan, R.S. 1995. Formation of cartilage-like spheroids by micromass cultures of murine C3H10T1/2 cells upon treatment with transforming growth factor-β 1. *Differentiation.* 59:25–34.
23. Yamamoto, A., et al. 2003. Suppression of arthritic bone destruction by adenovirus-mediated dominant-negative Ras gene transfer to synoviocytes and osteoclasts. *Arthritis Rheum.* 48:2682–2692.
24. Takayanagi, H., et al. 2000. Involvement of receptor activator of nuclear factor κB ligand/osteoclast differentiation factor in osteoclastogenesis from synoviocytes in rheumatoid arthritis. *Arthritis Rheum.* 43:259–269.
25. Tanaka, S., et al. 1998. Modulation of osteoclast function by adenovirus vector-induced epidermal growth factor receptor. *J. Bone Miner. Res.* 13:1714–1720.
26. Miyake, S., et al. 1996. Efficient generation of recombinant adenoviruses using adenovirus DNA-terminal protein complex and a cosmid bearing the full-length virus genome. *Proc. Natl. Acad. Sci. U. S. A.* 93:1320–1324.
27. Fujii, M., et al. 1999. Roles of bone morphogenetic protein type I receptors and Smad proteins in osteoblast and chondroblast differentiation. *Mol. Biol. Cell.* 10:3801–3813.
28. Enomoto-Iwamoto, M., et al. 2000. Hedgehog proteins stimulate chondrogenic cell differentiation and cartilage formation. *J. Bone Miner. Res.* 15:1659–1668.
29. Kamekura, S., et al. 2003. Establishment of novel experimental osteoarthritis models in mice. *J. Bone Miner. Res.* 18:S395.
30. van den Berg, W.B. 2001. Lessons from animal models of osteoarthritis. *Curr. Opin. Rheumatol.* 13:452–456.
31. Derynck, R., Zhang, Y., and Feng, X.H. 1998. Smads: transcriptional activators of TGF-β responses. *Cell.* 95:737–740.
32. Miyazono, K., Kusanagi, K., and Inoue, H. 2001. Divergence and convergence of TGF-β/BMP signaling. *J. Cell Physiol.* 187:265–276.
33. Watanabe, H., de Caestecker, M.P., and Yamada, Y. 2001. Transcriptional cross-talk between Smad, ERK1/2, and p38 mitogen-activated protein kinase pathways regulates transforming growth factor-β-induced aggrecan gene expression in chondrogenic ATDC5 cells. *J. Biol. Chem.* 276:14466–14473.
34. Miyazono, K. 1997. TGF-β receptors and signal transduction. *Int. J. Hematol.* 65:97–104.
35. Massague, J. 1998. TGF-β signal transduction. *Annu. Rev. Biochem.* 67:753–791.
36. de Crombrugghe, B., et al. 2000. Transcriptional mechanisms of chondrocyte differentiation. *Matrix Biol.* 19:389–394.
37. Akiyama, H., Chaboissier, M.C., Martin, J.F., Schedl, A., and de Crombrugghe, B. 2002. The transcription factor Sox9 has essential roles in successive steps of the chondrocyte differentiation pathway and is required for expression of Sox5 and Sox6. *Genes Dev.* 16:2813–2828.
38. Mi, Z., et al. 2003. Adverse effects of adenovirus-mediated gene transfer of human transforming growth factor beta 1 into rabbit knees. *Arthritis Res.* 5:R132–R139.
39. Nakamura, K., et al. 1999. p38 mitogen-activated protein kinase functionally contributes to chondrogenesis induced by growth/differentiation factor-5 in ATDC5 cells. *Exp. Cell Res.* 250:351–363.
40. Zhen, X., Wei, L., Wu, Q., Zhang, Y., and Chen, Q. 2001. Mitogen-activated protein kinase p38 mediates regulation of chondrocyte differentiation by parathyroid hormone. *J. Biol. Chem.* 276:4879–4885.
41. von der Mark, K., et al. 1995. Upregulation of type X collagen expression in osteoarthritic cartilage. *Acta Orthop. Scand. Suppl.* 266:125–129.
42. Scharstuhl, A., et al. 2003. Adenoviral overexpression of Smad-7 and Smad-6 differentially regulates TGF-β-mediated chondrocyte proliferation and proteoglycan synthesis. *Osteoarthritis Cartilage.* 11:773–782.
43. Hidaka, C., et al. 2003. Acceleration of cartilage repair by genetically modified chondrocytes over expressing bone morphogenetic protein-7. *J. Orthop. Res.* 21:573–583.
44. Lories, R.J., Derese, I., Ceuppens, J.L., and Luyten, F.P. 2003. Bone morphogenetic proteins 2 and 6, expressed in arthritic synovium, are regulated by proinflammatory cytokines and differentially modulate fibroblast-like synoviocyte apoptosis. *Arthritis Rheum.* 48:2807–2818.
45. Fukui, N., Zhu, Y., Maloney, W.J., Clohisy, J., and Sandell, L.J. 2003. Stimulation of BMP-2 expression by pro-inflammatory cytokines IL-1 and TNF-α in normal and osteoarthritic chondrocytes. *J. Bone Joint Surg. Am.* 85-A(Suppl. 3):59–66.
46. Pargellis, C., and Regan, J. 2003. Inhibitors of p38 mitogen-activated protein kinase for the treatment of rheumatoid arthritis. *Curr. Opin. Investig. Drugs.* 4:566–571.

 Related Commentary, page 805

PPARγ insufficiency enhances osteogenesis through osteoblast formation from bone marrow progenitors

Toru Akune,[1] Shinsuke Ohba,[2] Satoru Kamekura,[1] Masayuki Yamaguchi,[1] Ung-il Chung,[2] Naoto Kubota,[3] Yasuo Terauchi,[3] Yoshifumi Harada,[4] Yoshiaki Azuma,[4] Kozo Nakamura,[1] Takashi Kadowaki,[3] and Hiroshi Kawaguchi[1]

[1]Department of Orthopaedic Surgery, [2]Department of Tissue Engineering, and [3]Department of Metabolic Diseases, Faculty of Medicine, University of Tokyo, Tokyo, Japan. [4]Teijin Co., Tokyo, Japan.

Based on the fact that aging is associated with a reciprocal decrease of osteogenesis and an increase of adipogenesis in bone marrow and that osteoblasts and adipocytes share a common progenitor, this study investigated the role of PPARγ, a key regulator of adipocyte differentiation, in bone metabolism. Homozygous *PPARγ*-deficient ES cells failed to differentiate into adipocytes, but spontaneously differentiated into osteoblasts, and these were restored by reintroduction of the *PPARγ* gene. Heterozygous *PPARγ*-deficient mice exhibited high bone mass with increased osteoblastogenesis, but normal osteoblast and osteoclast functions, and this effect was not mediated by insulin or leptin. The osteogenic effect of PPARγ haploinsufficiency became prominent with aging but was not changed upon ovariectomy. The PPARγ haploinsufficiency was confirmed to enhance osteoblastogenesis in the bone marrow cell culture but did not affect the cultures of differentiated osteoblasts or osteoclast-lineage cells. This study demonstrates a PPARγ-dependent regulation of bone metabolism in vivo, in that PPARγ insufficiency increases bone mass by stimulating osteoblastogenesis from bone marrow progenitors.

Introduction

Osteoblasts and adipocytes share a common progenitor: multipotential mesenchymal stem cells in bone marrow (1–3). Accumulated evidence of the differentiation switching of these two cell lineages suggests that a large degree of plasticity exists between them and that the relationship is reciprocal (4–6). The clinical fact that a decrease in bone volume (BV) of age-related osteoporosis is accompanied by an increase in marrow adipose tissue (7–9) also implies the possible reciprocal relationship that is postulated to exist between the two differentiation pathways. The signal transduction pathways implicated in this process are therefore evaluated as potential targets for therapeutic intervention of osteoporosis. The molecular mechanism underlying the reciprocal relationship is not yet well understood, however, although several studies using strain-specific and KO murine models have begun to explore the relationship in vivo (10–15).

Several key transcription factors that function in the complex transcriptional cascade during adipocyte differentiation have been identified, including PPARγ and CCAAT enhancer-binding proteins (C/EBPs) (16). PPARγ is a ligand-activated transcription factor that belongs to the nuclear hormone receptor superfamily and functions as a heterodimer with a retinoid X receptor by binding to the PPAR responsive element (PPRE) within the promoters of the target genes (17–19). PPARγ is expressed early in the adipocyte differentiation program and is activated by long-chain fatty acids, peroxisome proliferators, and the thiazolidinedione class of antidiabetic agents (17–19). Most importantly, PPARγ plays requisite and sufficient roles in the regulation of adipocyte differentiation, because its overexpression in fibroblast cell lines initiates adipogenesis (20) and ES cells and embryonic fibroblastic cells from mice lacking *PPARγ* were unable to differentiate into adipocytes (21–23).

When one takes the results of the studies together, it is possible that PPARγ may contribute not only to adipogenesis, but also to osteogenesis in the bone marrow where bipotential precursors can differentiate to either adipocytes or osteoblasts. This study investigated the physiological role of PPARγ on the marrow cells and bone cells using in vivo morphological analyses and ex vivo cell culture systems. For the in vivo analysis, we used mice lacking the *PPARγ* gene, which we generated by gene targeting (22). Although the homozygous *PPARγ*-deficient (*PPARγ*$^{-/-}$) mice were embryonically lethal at 10.5–11.5 days after post coitum due to placental dysfunction, heterozygous *PPARγ*-deficient (*PPARγ*$^{+/-}$) mice developed normally. The heterozygotes led to a 50% reduction in PPARγ expression and exhibited resistance to high-fat diet–induced obesity and insulin resistance; however, on a standard diet they grew normally, without abnormalities in major organs such as brain, heart, liver, spleen, or kidney (22, 24). We show here that the homozygous *PPARγ*-deficient ES cells spontaneously differentiate into osteoblasts ex vivo and that PPARγ haploinsufficiency due to the heterozygous *PPARγ* deficiency resulted in enhanced bone formation with increased osteoblastogenesis from bone marrow progenitors both in vivo and ex vivo.

Methods

Animals. The generation of *PPARγ* gene-targeted mice was described previously (22). In each experiment, WT and *PPARγ*$^{+/-}$

Nonstandard abbreviations used: alkaline phosphatase (ALP); bone morphogenetic protein-2 (BMP-2); bone volume (BV); CCAAT enhancer-binding proteins (C/EBPs); computed tomography (CT); LDL receptor–related protein 5 (LRP5); leukemia inhibitory factor (LIF); M-CSF–dependent bone marrow macrophage (M-BMMϕ); receptor activator of nuclear factor κB ligand (RANKL); ovariectomy (OVX); PPAR responsive element (PPRE); tartrate-resistant acid phosphatase (TRAP); tissue volume (TV); type I collagen α1 chain (COL1A1).

Conflict of interest: The authors have declared that no conflict of interest exists.

Citation for this article: *J. Clin. Invest.* 113:846–855 (2004). doi:10.1172/JCI200419900.

mice littermates fed a standard diet were compared. All experiments were performed on male mice at 8 or 52 weeks of age, except for the ovariectomy (OVX) experiment in which female mice underwent surgical operation at 26 weeks and were analyzed at 30 weeks. All experiments were performed according to the protocol approved by the Animal Care and Use Committee of the University of Tokyo.

ES cell cultures. Mouse *PPARγ*$^{-/-}$ and WT ES cells were isolated from blastocysts generated by mating *PPARγ*$^{+/-}$ mice with each other, as previously described (25). ES cells were maintained in DMEM medium supplemented with 15% FBS, 200 mM L-glutamine, 100 μM β-mercaptoethanol, and 10^3 U/ml of leukemia inhibitory factor (LIF; Chemicon International, Temecula, California, USA). Differentiation of ES cells was induced by using a modified protocol, described previously (2, 26). In brief, after being trypsinized with 0.025% trypsin-EDTA, cells were plated onto a bacterial Petri dish in the absence of LIF and cultured with 100 nM all-*trans* retinoic acid for 5 days, with medium being replenished on day 3. The embryoid bodies were transferred to a gelatinized six-multiwell plate and allowed to adhere to the well with DMEM containing 10% FBS. For the analysis of osteogenic differentiation, cultures were maintained in the same condition without any additional supplements for 10 days, were fixed with 10% buffered formalin, and were incubated in the presence of 5% silver nitrate solution under an ultraviolet light for 10 minutes, then incubated for 5 minutes in the presence of 5% sodium thiosulfate solution (von Kossa staining). To discern the calcified nodules from the embryoid body, both of which are seen as black, the von Kossa-positive nodules that do not connect to the embryoid body in a well were counted. For the analysis of adipogenesis, the medium was supplemented with 1 μM troglitazone (Sankyo Pharmaceutical Co., Tokyo, Japan) for 10 days, fixed in 10 mM sodium periodate, 2% paraformaldehyde, 75 mM L-lysin dihydrochloride, and 37.5 mM sodium phosphate, and then stained in a filtered solution of 0.3% oil red O in 60% isopropanol for 15 minutes. The red-stained, lipid vacuole–containing cells in a well were counted. To rescue osteoblast and adipocyte differentiation of *PPARγ*$^{-/-}$ ES cells, the recombinant retrovirus vector carrying the *PPARγ* gene and empty vector were constructed as previously described (22). ES cells were infected with equal titers of each recombinant virus as described (20), with some modification.

Skeletal morphology and blood chemistry. A bone radiograph was taken with a soft x-ray apparatus (SOFTEX; CMB-2, Tokyo, Japan). A three-dimensional CT scan was taken using a composite x-ray analyzing system (NX-HCP; NS-ELEX Inc., Tokyo, Japan) and the trabecular bone area (percentage of BV per tissue volume [TV]) was measured on the computed tomography (CT) image. All histological analyses were carried out using WT and *PPARγ*$^{-/-}$ littermates as previously described (27). Parameters for the trabecular bone and the number of bone marrow adipocytes was measured in an area 1.2 mm in length from 0.5 mm below the growth plate at the proximal metaphysis of the tibiae. The number of adipocytes in this area was determined by counting that of oval vacuoles in the toluidine blue staining. The thickness of the growth plate was measured at the proximal tibiae. Serum insulin was measured by insulin immunoassay (Morinaga Institute of Biological Science, Yokohama, Japan), and leptin was assayed with the ELISA-based Quantikine M mouse leptin immunoassay kit (R&D Systems Inc., Minneapolis, Minnesota, USA).

Primary bone marrow cell cultures. Bone marrow cells were collected from long bones of 8-week-old *PPARγ*$^{-/-}$ and WT male littermates. Cells were plated at a density of 10^6 cells on a six-multiwell plate in α-MEM containing 10% FBS, with 1 μM troglitazone for the adipogenesis assay and with 50 μg/ml ascorbic acid and 10 mM β-glycerophosphate for osteogenesis assay. The oil red O staining was performed as mentioned above at 14 days of culture. For the alkaline phosphatase (ALP), cultured plates were rinsed with PBS, fixed in 100% ethanol at 10 days of culture, and stained with Tris-HCl–buffered solution (pH 9.0) containing naphthol AS-MX phosphate as a substrate and Fast Blue BB salt (Sigma-Aldrich, St. Louis, Missouri, USA) as a coupler. For the Alizarin red S staining, cultured plates were rinsed with PBS at 21 days of culture, fixed in 10% buffered formalin, and stained with 2% Alizarin red S (pH 4.0) (Sigma-Aldrich). The von Kossa staining was performed as mentioned above at 28 days of culture. For the growth curve assay, bone marrow cells derived from either WT or *PPARγ*$^{-/-}$ littermates were inoculated at a density of 10^7 cells per dish in 10-cm culture dishes in α-MEM containing 10% FBS, 50 μg/ml ascorbic acid, and 10 mM β-glycerophosphate, and then was cultured for 3 days. The adherent cells were then harvested and inoculated at a density of 3×10^5 cells/dish in 10-cm culture dishes and further cultured in the same medium. The number of cells per dish was counted 1, 2, 3, and 4 days after the seeding.

Real-time quantitative RT-PCR. Total RNA was extracted with an ISOGEN kit (Wako Pure Chemicals Industry Ltd., Osaka, Japan), according to the manufacturer's instructions, from ES cells cultured for 10 days after the embryoid bodies were transferred to gelatinized plates and from bone marrow cells cultured for 14 days after the seeding. One microgram of RNA was reverse-transcribed using a Takara RNA PCR Kit (AMV) ver. 2.1 (Takara Shuzo Co., Shiga, Japan) to make single-stranded cDNA. PCR was performed on an ABI Prism 7000 Sequence Detection System (Applied Biosystems Inc., Foster City, California, USA). The PCR reactions consisted of QuantiTect SYBR Green PCR Master Mix (QIAGEN, Tokyo, Japan), 0.3 μM specific primers, and 500 ng of cDNA. Relative levels of mRNA of a specific gene were calculated using the standard curve generated with cDNA dilutions, with normalization to actin as an internal control. PCR primers of specific genes used for amplification are available upon request.

Primary osteoblastic cell cultures. Osteoblastic cells were isolated from calvariae of neonatal WT and *PPARγ*$^{-/-}$ littermates as previously described (27). For the cell proliferation assay, cells were inoculated at a density of 10^4 cells/well in a 24-multiwell plate, cultured in the same medium for 48 hours, and deprived of serum for 12 hours before adding the experimental medium with and without troglitazone (1 μM) or FGF-2 (1 nM; Kaken Pharmaceutical Co., Chiba, Japan). Incorporation of [^{3}H]-thymidine (1 μCi/ml in the medium) added for the final 3 hours was measured after 24 hours of culture. For ALP activity measurement, cells were inoculated at a density of 10^4 cells/well in a 24-multiwell plate and cultured in α-MEM containing 10% FBS and 50 μg/ml ascorbic acid with and without troglitazone (1 μM) or bone morphogenetic protein-2 (BMP-2; 30 ng/ml; Yamanouchi Pharmaceutical Co., Tokyo, Japan). At 14 days of culture, cells were sonicated in 10 mM Tris-HCl buffer (pH 8.0) containing 1 mM $MgCl_2$ and 0.5% Triton X-100. ALP activity in the lysate was measured using a Wako ALP kit (Wako Pure Chemicals Industry Ltd.), and the protein content was determined using a BCA protein assay reagent (Pierce Chemical Co., Rockford, Illinois, USA). For Alizarin red S and von Kossa stainings, cells were inoculated at a density of 5×10^4 cells/well in a six-multiwell plate in α-MEM containing 10% FBS, 50 μg/ml ascorbic acid, and 10 mM β-glyc-

erophosphate, and were stained at day 21 and 28, respectively, as mentioned above. Difference in maturity between the bone marrow cells and the calvarial osteoblasts was examined by the calcified nodule formation determined by Alizarin red S staining and the osteocalcin expression determined by real-time PCR analysis.

Assays for osteoclastic cells. Tartrate-resistant acid phosphatase-positive (TRAP-positive) multinucleated osteoclasts were generated by coculturing osteoblastic cells (10^4 cells/well) and bone marrow cells (5×10^5 cells/well) derived from either WT or *PPARγ*$^{+/-}$ littermates, as mentioned above, in a 24-multiwell plate in α-MEM containing 10% FBS for 6 days with and without $1,25(OH)_2D_3$ (10 nM), prostaglandin E_2 (100 nM), and IL-11 (10 ng/ml). Cells positively stained for TRAP containing more than three nuclei were counted as osteoclasts. To determine bone resorption activity, osteoclasts formed by the coculture on 0.24% collagen gel coated on 100-mm dishes were digested with 0.2% collagenase solution, and a 1:50 aliquot including osteoclasts was seeded on a dentine slice. After 48 hours of culture in α-MEM containing 10% FBS, the total area of pits stained with 0.5% toluidine blue was evaluated using an image analyzer. To study the role of PPARγ intrinsic to osteoclastic cells, we used the M-CSF–dependent bone marrow macrophage (M-BMMϕ) culture system as described previously (28). Briefly, bone marrow cells from WT or *PPARγ*$^{+/-}$ mice were seeded at a density of 3×10^5 cells/well in a 24-multiwell plate and cultured in α-MEM containing 10% FBS with M-CSF (100 ng/ml). After culturing for 3 days, adherent cells (M-BMMϕ) were further cultured with M-CSF (100 ng/ml) and soluble receptor activator of nuclear factor κB ligand (RANKL) (100 ng/ml) for 3 days. TRAP-positive osteoclasts were counted. To determine the survival, osteoclasts generated as above were deprived of M-CSF/soluble RANKL and cultured for an additional 48 hours. At 3, 6, 12, 24, and 48 hours, the TRAP-positive and trypan blue–negative osteoclasts were counted.

Statistical analysis. Means of groups were compared by ANOVA, and significance of differences was determined by post-hoc testing using Bonferroni's method.

Results

Osteogenesis is enhanced in the homozygous PPARγ-deficient ES cell culture. To examine the involvement of the PPARγ signaling in fat and bone metabolism, we first compared the adipogenesis and osteogenesis in

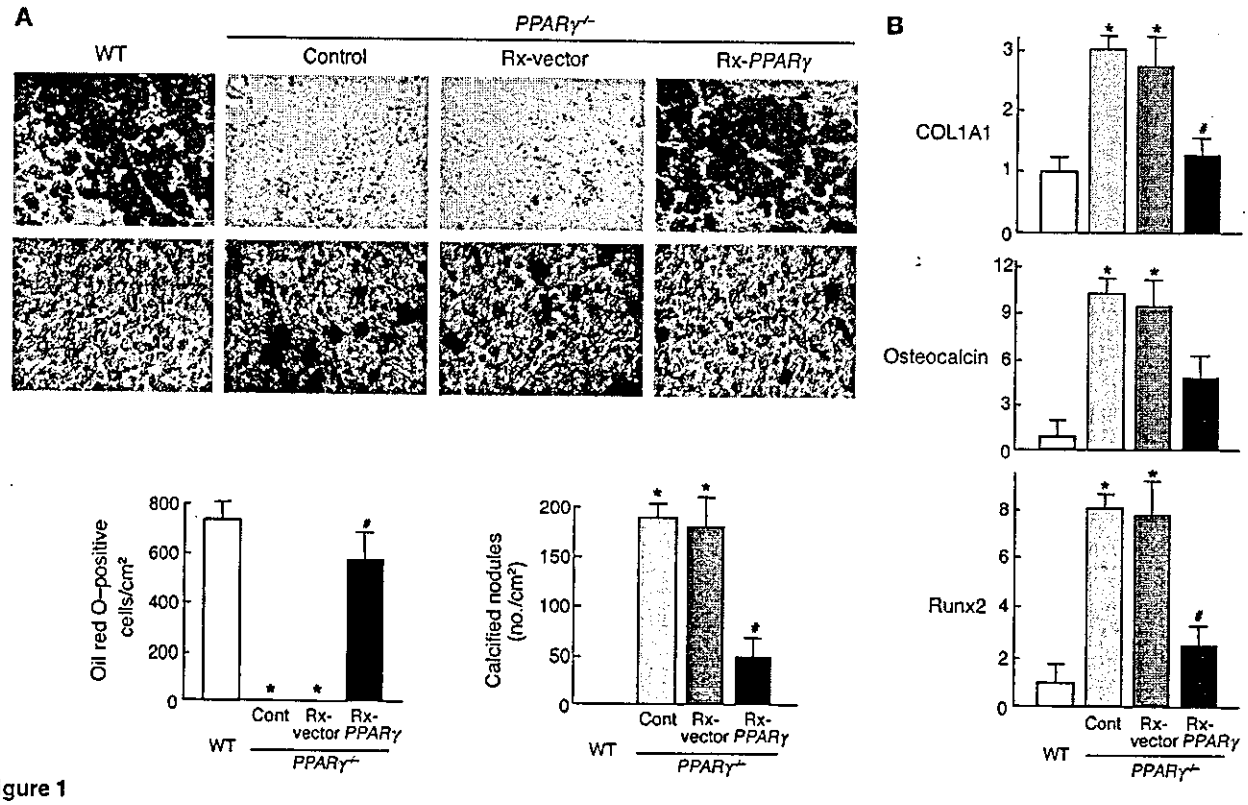

Figure 1

Adipogenesis and osteogenesis in the mouse ES cell cultures of homozygous *PPARγ*-deficient (*PPARγ*$^{-/-}$) and WT genotypes. As a rescue experiment, PPARγ was reintroduced into *PPARγ*$^{-/-}$ ES cells using a retrovirus vector carrying the *PPARγ* gene (Rx-*PPARγ*) or the same retrovirus vector without the *PPARγ* gene (Rx-vector) as a control. (**A**) The upper row shows the adipogenesis determined by the oil red O staining of the ES cell culture in DMEM/10% FBS with troglitazone. The number of oil red O–positive cells stained in red was counted and shown in the left graph as the cells per square centimeter. The images in the lower row indicate the osteogenesis determined by the von Kossa staining of the ES cell culture in DMEM/10% FBS without any osteogenic supplements. The number of von Kossa–positive calcified nodules stained in black was counted and shown in the right graph as the number per square centimeter. Scale bar: 20 μm. (**B**) Relative mRNA levels of the marker genes for osteoblasts — COL1A1, osteocalcin and Runx2 — determined by real-time quantitative RT-PCR 10 days after the embryoid bodies were transferred to a gelatinized six-multiwell plate in DMEM/10% FBS without any osteogenic supplements. The ordinate axis indicates the relative amount of mRNA as compared with that of WT. Data are expressed as means (bars) ± SEMs (error bars) for eight wells per group. *Significant difference from the WT culture, $P < 0.01$. #Significant restoration by Rx-*PPARγ* as compared with the control *PPARγ*$^{-/-}$ and *PPARγ*$^{-/-}$ plus Rx-vector cultures; $P < 0.01$. Cont, control.

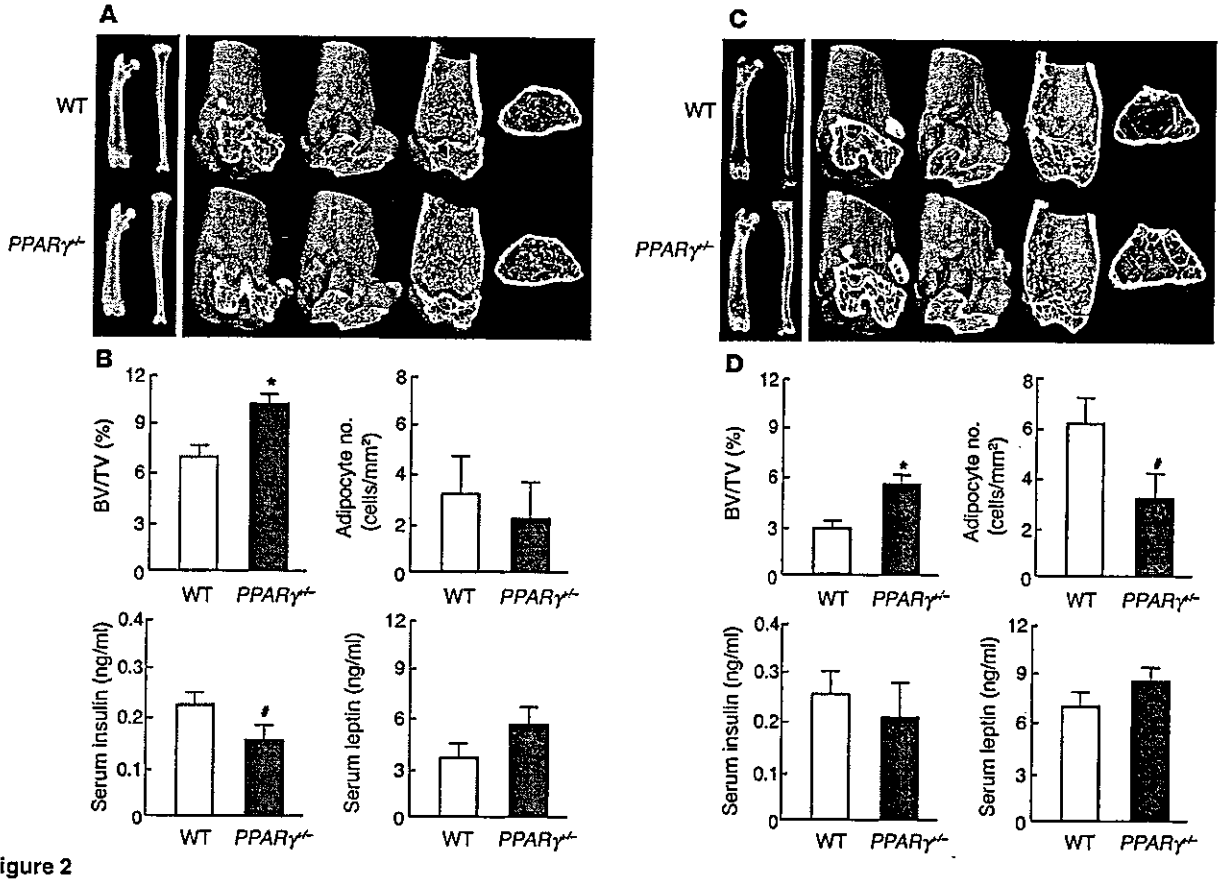

Figure 2

Radiological analysis and blood chemistry of heterozygous *PPARγ*-deficient (*PPARγ*$^{+/-}$) and WT littermates at 8 weeks (**A** and **B**) and 52 weeks (**C** and **D**) of age. (**A** and **C**) Plain x-ray images of femora and tibiae (left) and three-dimensional CT images of distal femora (right) of representative *PPARγ*$^{+/-}$ and WT littermates. (**B** and **D**) Trabecular BV expressed as percentage of total tissue volume (BV/TV [%]) at the distal femora was measured on the CT image. The number of adipocytes in the bone marrow, measured histologically, is shown here for collation with the BV/TV data. Insulin and leptin levels in serum taken just before the sacrifice were quantified using immunoassay kits. Data are expressed as means (bars) ± SEMs (error bars) for eight mice per group for *PPARγ*$^{+/-}$ and WT mice. Significant difference from WT: $^{*}P < 0.01$, $^{\#}P < 0.05$.

the cultures of ES cells between *PPARγ*$^{-/-}$ and WT (WT or *PPARγ*$^{+/+}$) genotypes isolated from blastocysts generated by mating *PPARγ*$^{+/-}$ mice (Figure 1A). In the presence of troglitazone, a thiazolidinedione that is a potent ligand of PPARγ, a substantial amount of oil red O–positive adipocytes was formed from WT ES cells, whereas adipogenesis was not seen in the *PPARγ*$^{-/-}$ ES cell culture (Figure 1A, upper row of photographs). To confirm the direct association between PPARγ and adipogenesis, PPARγ was reintroduced into *PPARγ*$^{-/-}$ ES cells using a retrovirus vector carrying the *PPARγ* gene (Rx-*PPARγ*). Adipogenesis was restored to the level similar to that of WT culture, although introduction of the same retrovirus vector without the *PPARγ* gene (Rx-vector) did not affect it. We then examined the osteogenesis in the *PPARγ*$^{-/-}$ and WT ES cell cultures. Surprisingly, in DMEM/10% FBS without osteogenic supplements such as dexamethasone, β-glycerophosphate, ascorbic acid, or BMP, the formation of von Kossa–positive bone nodules was potently induced in the *PPARγ*$^{-/-}$ ES cell culture, while this was not seen at all in the WT culture (Figure 1A, lower row of photographs). Quantitative analysis of the mRNA levels by the real-time RT-PCR method revealed that the marker genes for osteoblasts — type I collagen α1 chain (COL1A1), osteocalcin, and Runx2 — were upregulated in the *PPARγ*$^{-/-}$ ES cell culture as compared with the WT culture (Figure 1B). Reintroduction of PPARγ into the *PPARγ*$^{-/-}$ culture by Rx-*PPARγ* significantly decreased the nodule formation and osteogenic marker gene expressions, while the control Rx-vector altered neither (Figure 1, A and B). When one takes these results together, the observed mirror image regulations between adipogenesis and osteogenesis by loss and gain of the PPARγ function suggest a switching mechanism between the two differentiation pathways from common progenitors through the PPARγ signaling.

PPARγ haploinsufficiency leads to high bone mass in vivo. To learn the effect of the PPARγ insufficiency in vivo, we analyzed the bones of *PPARγ*$^{+/-}$ mice because the homozygous deficient fetuses died too early for their skeletal analyses to be performed. *PPARγ*$^{+/-}$ mice showed normal weight gain without visible general lipodystrophy on a standard diet during the observation period of up to 52 weeks of age. The lengths of the trunk and long bones were also similar to those of WT littermates, indicating that PPARγ is not involved in the regulation of skeletal growth. X-ray and three-dimensional CT analyses of femora and tibiae, however, revealed that *PPARγ*$^{+/-}$ mice showed about 40% higher trabecular bone mass than WT littermates at 8 weeks of age (Figure 2, A and B).

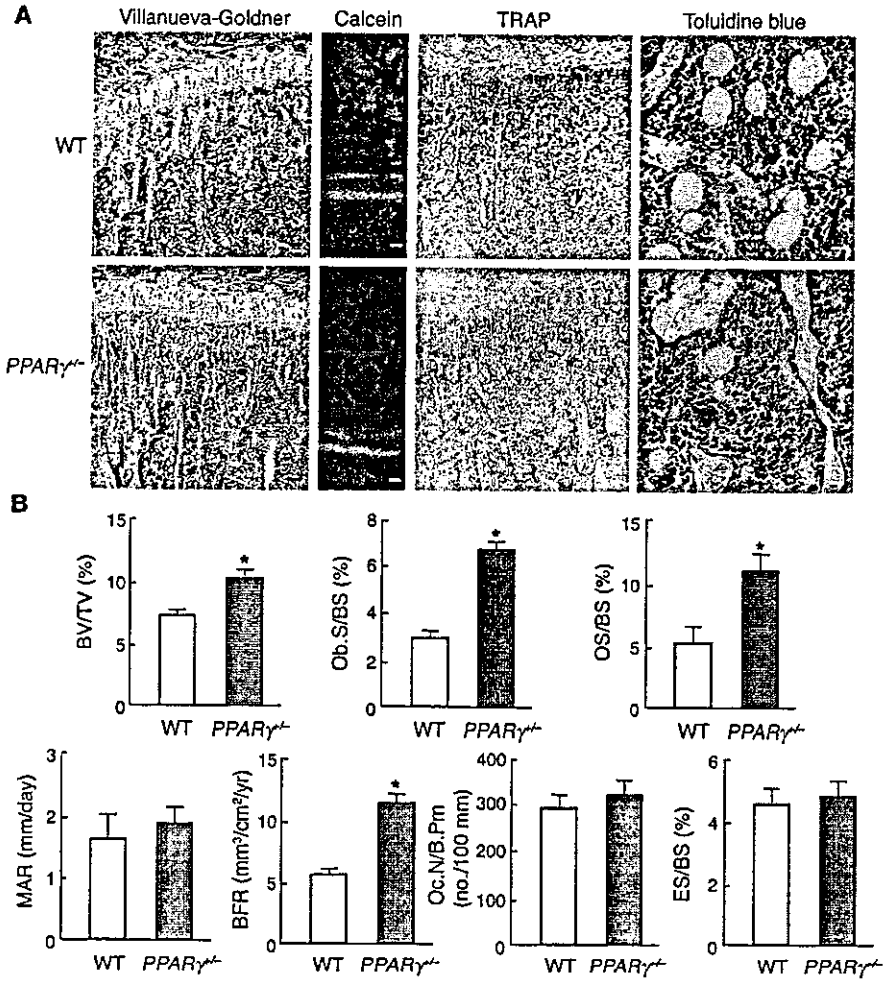

Figure 3
Histological analysis of the proximal tibiae of *PPARγ*$^{+/-}$ and WT littermates. (A) Histological features at proximal tibiae of *PPARγ*$^{+/-}$ and WT littermates. Villanueva-Goldner staining, calcein double labeling, and TRAP staining were done at 8 weeks; toluidine blue staining was done at 52 weeks of age. In Villanueva-Goldner staining, mineralized bone is stained green and unmineralized bone osteoid red; scale bar: 100 μm. In calcein double labeling, the mineralization front is stained as a green line; scale bar: 10 μm. In TRAP staining, TRAP-positive osteoclasts are stained red; scale bar: 100 μm. In toluidine blue staining, adipocytes are observed as oval vacuoles; scale bar: 50 μm. (B) Histomorphometric parameters at 8 weeks of age. Ob.S/BS, percentage of bone surface covered by cuboidal osteoblasts; OS/BS, percentage of bone surface covered by osteoid; MAR, mineral apposition rate; BFR, bone formation rate expressed by MAR times percentage of bone surface exhibiting double labels plus one-half single labels; Oc.N/B.Pm, number of mature osteoclasts in 100 mm of bone perimeter; ES/BS, percentage of eroded surface. Data are expressed as means (bars) ± SEMs (error bars) for eight mice per group for *PPARγ*$^{+/-}$ and WT mice. *Significant difference from WT, $P < 0.01$.

Contrarily, the number of adipocytes in the bone marrow determined as described below tended to be lower in the *PPARγ*$^{+/-}$ long bones compared with WT (Figure 2B). Similar changes of bone and fat were also seen in vertebral bodies (data not shown). To examine the involvement of systemic factors that are known to be related to bone and fat metabolism, the serum levels of insulin and leptin were compared between the two mouse genotypes. *PPARγ*$^{+/-}$ mice showed lower, although not significantly lower, serum insulin level and higher leptin level than WT littermates as reported previously (22, 29). Since insulin is known to be osteogenic (30), whereas leptin is antiosteogenic (11, 13, 31), neither of the changes in these hormones could explain the increased bone mass in *PPARγ*$^{+/-}$ mice.

Because age-related osteoporosis is known to be accompanied by reciprocal increase of bone marrow adipocytes (7–9), we further compared the bones of *PPARγ*$^{+/-}$ and WT littermates at 52 weeks of age (Figure 2, C and D). The BV of femora and tibiae was decreased in both mouse genotypes at this age as compared with that at 8 weeks; however, the difference of BV between *PPARγ*$^{+/-}$ and WT became more prominent at 52 weeks than at 8 weeks (95% versus 40%, respectively). The number of bone marrow adipocytes, which are shown as oval vacuoles by the toluidine blue staining (Figure 3A, right), was significantly decreased in *PPARγ*$^{+/-}$ mice at this age. This tendency was similarly observed in vertebral bodies (data not shown). Both insulin and leptin levels at this old age showed patterns similar to those at 8 weeks, although significant differences between the genotypes were not seen.

PPARγ haploinsufficiency leads to osteoblastogenesis in vivo. We further performed histological analyses of the proximal tibiae of 8-week-old *PPARγ*$^{+/-}$ mice. Villanueva-Goldner staining indicated increases of trabecular bones stained in green and osteoid surface stained in red in *PPARγ*$^{+/-}$ mice as compared with WT littermates; however, bone formation by individual osteoblasts determined by the calcein double labeling and the number of TRAP-positive osteoclasts was similar for the two groups (Figure 3A). Bone histomorphometric analyses (Figure 3B) confirmed the increase of BV by PPARγ haploinsufficiency to be about 40%. Among bone formation parameters, osteoblast surface and osteoid surface, both representative of the number of osteoblasts, were more than double in *PPARγ*$^{+/-}$ than in WT littermates, while the mineral apposition rate that reflects the bone formation ability of individual osteoblasts did not differ between them. Consequently, bone formation rate that is determined by the number and the function of osteoblasts became about twice that by PPARγ haploinsufficiency. Bone resorption parameters, osteoclast number, and eroded surface did not differ between *PPARγ*$^{+/-}$ and WT mice. Taking these histologi-

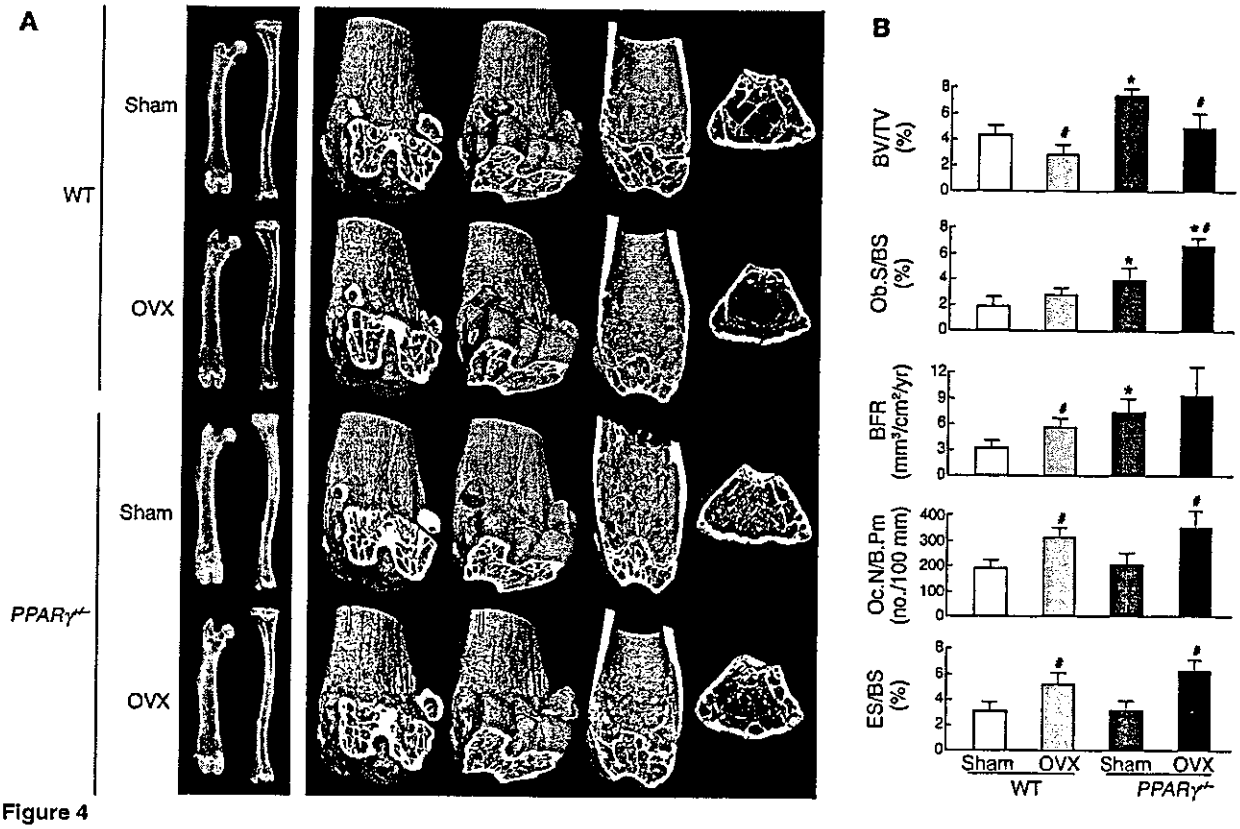

Figure 4

Radiological and histomorphometric analyses of OVX and sham-operated (Sham) female littermates of *PPARγ*$^{+/-}$ and WT genotypes. Female mice underwent surgical operation at 26 weeks and were analyzed at 30 weeks of age. (**A**) Plain x-ray images of femora and tibiae (left) and three-dimensional CT images of distal femora (right) of representative mice. (**B**) Histomorphometric parameters. Data are expressed as means (bars) ± SEMs (error bars) for eight mice per group for *PPARγ*$^{+/-}$ and WT mice. *Significant difference from WT, $P < 0.01$. #Significant difference from sham, $P < 0.05$.

cal observations together, *PPARγ*$^{+/-}$ mice exhibited high bone mass with increased osteoblastogenesis but normal osteoblast and osteoclast functions. The thickness of the growth plate at the proximal tibiae was not different between *PPARγ*$^{+/-}$ and WT littermates (80.4 ± 9.6 and 82.7 ± 10.3 μm, mean ± SEM of eight mice each, respectively), confirming that PPARγ signaling is not important for bone growth through chondrocyte functions.

PPARγ haploinsufficiency does not affect bone loss by OVX. To investigate the involvement of the PPARγ signaling in the mechanism of bone loss by estrogen deficiency, OVX or sham operation was undertaken on 26-week-old female *PPARγ*$^{+/-}$ and WT littermates, and BV was compared 4 weeks after the operation. X-ray and three-dimensional CT analyses of femora and tibiae suggested that both *PPARγ*$^{+/-}$ and WT mice showed similar bone loss by OVX (Figure 4A). Histomorphometric analyses (Figure 4B) showed that BV was about 30% decreased by OVX in both *PPARγ*$^{+/-}$ and WT mice. These decreases were accompanied by increases in bone formation and bone resorption parameters, indicating a state of high bone turnover, in both genotypes. Hence, PPARγ haploinsufficiency did not affect the change of bone metabolism induced by OVX, suggesting that the PPARγ signaling does not contribute to osteopenia caused by estrogen deficiency.

PPARγ haploinsufficiency leads to osteoblastogenesis from cultured bone marrow cells. To investigate the cellular mechanism underlying the abnormality in the bone of *PPARγ*$^{+/-}$ mice, ex vivo cultures of bone marrow cells derived from long bones were performed. We first compared the cell proliferation determined by the growth curve for 4 days and found no difference between *PPARγ*$^{+/-}$ and WT marrow cells (Figure 5A). Adipogenesis from marrow cells in the presence of troglitazone was confirmed to be inhibited by PPARγ haploinsufficiency, however, since the number of oil red O–positive adipocytes was decreased in the *PPARγ*$^{+/-}$ culture to about half that of the WT culture (Figure 5B). We further examined osteoblastogenesis in the bone marrow cell culture by comparing the numbers of colonies positively stained with ALP, Alizarin red S, and von Kossa (Figure 5C). All colonies were markedly increased in the *PPARγ*$^{+/-}$ culture as compared with the WT culture, indicating the increase of osteoblastogenesis from bone marrow progenitors by PPARγ haploinsufficiency.

To further investigate the regulation of expression of genes related to bone metabolism by PPARγ haploinsufficiency, we compared mRNA levels of key or marker molecules for adipocyte and osteoblast differentiations between *PPARγ*$^{+/-}$ and WT bone marrow cells (Figure 5D). As expected, PPARγ expression was reduced in the *PPARγ*$^{+/-}$ marrow cells compared with the WT. The levels of expression of other key factors for adipocyte differentiation, C/EBP-β and C/EBP-δ, in the *PPARγ*$^{+/-}$ marrow cells were comparable to those of WT, indicating that PPARγ was not essential for induction of these C/EBPs; contrarily, C/EBP-α was significantly reduced. Based on previous observations (16, 17, 22, 32, 33) and these results, it appears that C/EBP-β and C/EBP-δ lie upstream of PPARγ, while C/EBP-α is

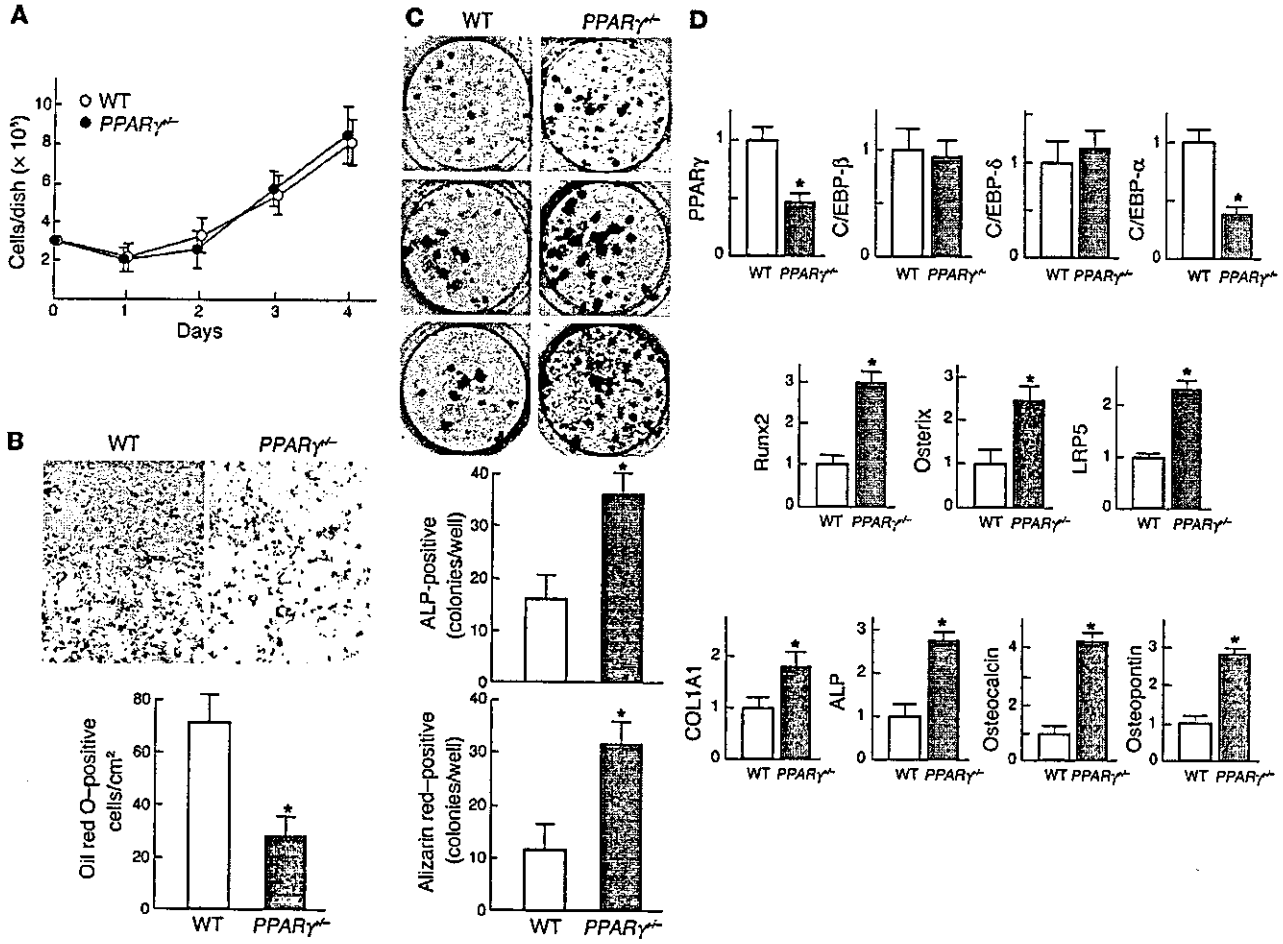

Figure 5

Adipogenesis and osteogenesis in the cultures of bone marrow cells from *PPARγ*$^{-/-}$ and WT littermates. (**A**) Growth curves of bone marrow cells isolated from *PPARγ*$^{-/-}$ and WT mice. The adherent bone marrow cells were inoculated at a density of 3×10^5 cells/dish in 10-cm culture dishes. The cells per dish were counted at 1, 2, 3, and 4 days of culture. Data are expressed as means (symbols) ± SEMs (error bars) for eight dishes per group. (**B**) Adipogenesis determined by oil red O staining in the culture of bone marrow cells in α-MEM/10% FBS with troglitazone. The graph indicates the number of positive cells per square centimeter. (**C**) Osteogenesis determined by ALP (upper row), Alizarin red (middle row), and von Kossa (lower row) stainings in the culture of bone marrow cells in α-MEM/10% FBS with ascorbic acid and β-glycerophosphate. The graphs below indicate the number of ALP-positive (upper) and Alizarin red–positive (lower) colonies per well. Data are expressed as means (bars) ± SEMs (error bars) for eight wells per group (**B** and **C**). *Significant difference from the WT culture, $P < 0.01$. (**D**) Expression of key molecules for adipogenesis (PPARγ, C/EBP-β, C/EBP-δ, and C/EBP-α) and osteogenesis (Runx2, osterix, and LRP5), and marker proteins for osteogenesis (COL1A1, ALP, osteocalcin, and osteopontin) determined by quantitative RT-PCR in the bone marrow cells at 14 days of culture under the conditions above. The ordinate axis indicates the relative amount of mRNA as compared with that of WT.

regulated, at least in part, downstream of PPARγ. Regarding osteogenic factors, expressions of the putative central determinants of major pathways for osteoblast differentiation, Runx2 (34), osterix (35), and LDL receptor-related protein 5 (LRP5) (36), were increased in the *PPARγ*$^{-/-}$ culture as compared with WT, indicating that the PPARγ signaling directly or indirectly impacts these major pathways for osteoblast differentiation. Expressions of matrix proteins representing osteogenesis, COL1A1, ALP, osteocalcin, and osteopontin, were also higher in the *PPARγ*$^{-/-}$ culture than in the WT culture, which was consistent with the in vivo histomorphometric data showing high bone mass with increased osteoblastogenesis.

When we examined the proliferation, differentiation, and matrix synthesis of cultured calvarial osteoblasts, which we confirmed to be more mature than bone marrow cells, none of them showed a difference between *PPARγ*$^{-/-}$ and WT mice (data not shown). This indicates that PPARγ haploinsufficiency affects only marrow progenitors, but not cells that are more committed to osteoblastic lineage. Furthermore, studies using the coculture system of marrow cells/calvarial osteoblasts and the M-BMMϕ culture system (28, 37) also failed to show difference of differentiation, bone-resorbing activity, or survival of the osteoclastic cells, suggesting that PPARγ is not important for osteoclast functions.

Discussion

Osteoblastogenesis was upregulated not only in the *PPARγ*$^{-/-}$ bone in vivo, but also in the cultures of *PPARγ*$^{-/-}$ ES cells and *PPARγ*$^{-/-}$

primary bone marrow cells. Considering that the former culture was performed in the absence of any osteogenic stimulation, under which condition no WT stem cells can differentiate into osteoblasts, the intrinsic PPARγ signaling seems to function as a potent suppressor of commitment and differentiation to the osteoblastic lineage. Its molecular mechanism remains unclear, however. A previous report showed that a stable transfection of PPARγ and its activation with a thiazolidinedione-suppressed Runx2, type I collagen, and osteocalcin syntheses in the culture of a stromal cell line (38). Although the present study also showed that steady-state mRNA levels of the key molecules for osteoblast differentiation, Runx2, osterix, and LRP5, were upregulated in primary cultured marrow cells with PPARγ haploinsufficiency (Figure 5D), whether this is transcriptional regulation or secondary to the increase in cells of osteoblast lineage in the culture is unknown. The predicted region of the PPARγ-responsive element PPRE (TGACCTnTGACCT) has not been identified in the promoter of these genes and was not found by our genomic search, at least in the region between 4.0 kb upstream and 0.5 kb downstream of the transcriptional start point of *runx2* (GenBank accession number NT 039655), *osterix* (NT 039621), and *lrp5* (NT 039684) genes. It should, however, also be noted that several reports have indicated that PPARγ regulates gene expression independently of PPRE, that is, by interfering with the function of AP-1, signal transducer and activator of transcription 1 (STAT1), and NF-κB (39), or by inhibiting the function of GHP-1, a transcription factor implicated in pituitary-specific gene expression (40). The AP-1 family members may possibly play a role in the mechanism, especially for mesenchymal cells. Activation of PPARγ is reported to suppress *c-fos* expression (41). Another AP-1 family member, DeltaFosB, is known to be a positive regulator of osteoblast differentiation, and the transgenic mouse leads to postnatal high bone mass with increased osteoblastogenesis and decreased adipogenesis in bone marrow (12). Another possible molecular mechanism is the interaction of PPARγ with the TGF-β/Smad3 signaling, which inhibits osteoblast differentiation (42, 43). Since Smad3 is reported to interact physically with Runx2 (42) and PPARγ (44), the interference by PPARγ with the Smad3 inhibition of Runx2 might be involved in the switching mechanism between adipocyte and osteoblast differentiation. The interaction of PPARγ with Wnt signaling might be another issue to pursue. The canonical Wnt pathway, likely mediated by Wnt10b, is known to maintain preadipocytes in an undifferentiated state through stabilization of cytosolic β-catenin (45, 46). Since activation of PPARγ with troglitazone is not sufficient to repress expression of Wnt10b, Wnt signaling might lie upstream of PPARγ. Recently, in addition to LRP5, which is a coreceptor of Wnt, the canonical Wnt-signaling molecules β-catenin and glycogen synthase kinase-3β have been reported to stimulate osteoblast differentiation (47, 48), indicating a switching between adipogenesis and osteogenesis by the Wnt signaling. Further studies on functional interaction of PPARγ with the transcriptional and signaling molecules above will elucidate the switching mechanism between the two differentiation pathways from common progenitors.

PPARγ may also inhibit osteogenesis indirectly through its stimulation of adipogenesis from marrow progenitors that can give rise to either osteoblasts or adipocytes. In fact, many experimental models have provided substantial evidence for this reciprocal relationship between cell lineages (6, 10–15), and there is little doubt that adipogenesis increases as BV decreases, suggesting that marrow adipogenesis has important implications in osteogenic disorders (7–9). Evidence of the transdifferentiation of stromal cells actually suggests a large degree of plasticity between osteoblasts and adipocytes (4, 49), although it is not clear at what point the phenotype of these multipotential cells becomes committed to either osteoblast or adipocyte differentiation. Since differentiated osteoblasts indicated by osteocalcin expression are reported to undergo adipogenic differentiation (4), it is possible that the reciprocal relationship between osteogenesis and adipogenesis may, at least in part, be due to the transdifferentiation between rather differentiated cells of the two lineages. To determine the role of PPARγ in more differentiated osteoblastic cells than bone marrow cells, we used calvarial cells whose spontaneous differentiation is known to follow not only the osteogenic pathway but also the adipogenic pathway (49). Despite the existence of PPARγ expression in these cells as well, its haploinsufficiency did not affect the cell functions, suggesting that PPARγ signaling may be involved in the earlier, but not the later, stage of relationship between the two cell lineages.

Hormones regulating bone and fat metabolisms include insulin and leptin, both of which are known to be related to the PPARγ signaling. Insulin is known to play important anabolic roles in bone (30), and deficiency of insulin signaling is associated with osteopenia both in mice and humans (27, 50–52). A series of reports demonstrated that leptin, a well-known anorexigenic hormone secreted by adipocytes (53), also shows antiosteogenic action centrally through the hypothalamic and sympathetic nervous systems (11, 13, 31). In the present study, neither insulin nor leptin seemed to mediate the high bone mass in *PPARγ*$^{+/-}$ mice, since the serum levels of these hormones were, quite unexpectedly, the opposite of those causing osteogenic functions. PPARγ activation is known to cause insulin sensitivity, thus *PPARγ*$^{+/-}$ mice were assumed to develop insulin resistance; however, the serum insulin level was normal or somewhat decreased as previously reported (22, 29). This appears, at least in part, due to hypersecretion of leptin, which was also unexpected, given that the marrow adipocytes, a positive regulator of leptin expression, were decreased in *PPARγ*$^{+/-}$ mice. Our previous studies clearly demonstrated that cultured primary adipocytes from *PPARγ*$^{+/-}$ mice expressed and secreted increased levels of leptin as compared with those from WT (22, 29). In this respect, since leptin is known to have a functional PPRE whose activity is suppressed by PPARγ activation in adipocytes (54, 55), it is likely that the increased level of leptin is due to a partial release from the suppressive effect of PPARγ on leptin gene transcription by loss of one *PPARγ* allele.

Age-related bone loss has been suggested to be attributable to increased adipogenesis at the expense of osteoblastogenesis (7–9). Indeed, studies of SAMP6 mice, a murine model of age-related osteopenia, have established a tight association between osteopenia and enhanced adipogenesis (10, 15). The fact that the effects of PPARγ haploinsufficiency on both the increase in bone volume and the decrease in adipocytes were stronger at 52 weeks than at 8 weeks suggests the involvement of the PPARγ signaling in the pathophysiology of human age-related osteoporosis. In fact, our preliminary examination of the bone marrow specimen from patients with femoral neck fracture actually showed increases of both the PPARγ mRNA level and fat mass in older patients (data not shown) as compared with those in younger patients, although the causality between PPARγ level and adipogenesis remains unknown since adipocytes can be both the source and the target

of PPARγ. An association study between bone density and a genetic polymorphism of *PPARγ* in postmenopausal women implies the involvement of PPARγ in bone loss, although the functional relevance remains unclear (56). We should, however, keep in mind that there are two distinct factors that determine involutional osteoporosis: a rapid bone loss after menopause as a result of estrogen withdrawal and a gradual age-related bone loss thereafter (57). From the present study showing that PPARγ insufficiency did not affect bone loss by OVX, PPARγ may not be involved in the former stage, but may play a role in the latter. To confirm the involvement of PPARγ in human osteoporosis, the next task ahead of us will be to perform a genetic association study with stratified analysis by age and menopausal state, and more importantly, to use a cohort population.

We conclude herein that PPARγ haploinsufficiency leads to the increase of bone mass by stimulating osteoblastogenesis from bone marrow progenitors without affecting differentiated osteoblasts or osteoclast lineage cells. Based on the present and previous evidence presented, we believe that PPARγ may be a novel target for therapeutic intervention of osteopenic disorders, although the mechanism remains to be clarified. Appropriate functional antagonism of PPARγ may provide a potentially novel approach to increasing bone formation and therefore, as a stand-alone therapy or in combination with an antiresorptive medication, may provide more efficacious prevention or treatment of osteoporosis.

Acknowledgments

We thank the hard tissue research team at Kureha Chemical Co. for technical assistance. We are grateful to Bruce M. Spiegelman for the pBabe-mPPARγ2-puro vector. This work was supported by Grants-in-Aid for Scientific Research from the Japanese Ministry of Education, Culture, Sports, Science, and Technology (1370303) and the ONO Medical Research Foundation.

Received for publication August 28, 2003, and accepted in revised form January 6, 2004.

Address correspondence to: Hiroshi Kawaguchi, Department of Orthopaedic Surgery, Faculty of Medicine, University of Tokyo, Hongo 7-3-1, Bunkyo-ku, Tokyo 113-8655, Japan. Phone: 81-33815-5411 ext. 30473 or 33376; Fax: 81-33818-4082; E-mail: kawaguchi-ort@h.u-tokyo.ac.jp.

1. Beresford, J.N. 1989. Osteogenic stem cells and the stromal system of bone and marrow. *Clin. Orthop.* 240:270–280.
2. Pittenger, M.F., et al. 1999. Multilineage potential of adult human mesenchymal stem cells. *Science.* 284:143–147.
3. Bennett, J.H., Joyner, C.J., Triffitt, J.T., and Owen, M.E. 1991. Adipocytic cells cultured from marrow have osteogenic potential. *J. Cell Sci.* 99:131–139.
4. Nuttall, M.E., Patton, A.J., Olivera, D.L., Nadeau, D.P., and Gowen, M. 1998. Human trabecular bone cells are able to express both osteoblastic and adipocytic phenotype: implications for osteopenic disorders. *J. Bone Miner. Res.* 13:371–382.
5. Park, S.R., Oreffo, R.O., and Triffitt, J.T. 1999. Interconversion potential of cloned human marrow adipocytes in vitro. *Bone.* 24:549–554.
6. Beresford, J.N., Bennett, J.H., Devlin, C., Leboy, P.S., and Owen, M.E. 1992. Evidence for an inverse relationship between the differentiation of adipocytic and osteogenic cells in rat marrow stromal cell cultures. *J. Cell Sci.* 102:341–351.
7. Meunier, P., Aaron, J., Edouard, C., and Vignon, G. 1971. Osteoporosis and the replacement of cell populations of the marrow by adipose tissue. A quantitative study of 84 iliac bone biopsies. *Clin. Orthop.* 80:147–154.
8. Burkhardt, R., et al. 1987. Changes in trabecular bone, hematopoiesis and bone marrow vessels in aplastic anemia, primary osteoporosis, and old age: a comparative histomorphometric study. *Bone.* 8:157–164.
9. Rozman, C., et al. 1989. Age-related variations of fat tissue fraction in normal human bone marrow depend both on size and number of adipocytes: a stereological study. *Exp. Hematol.* 17:34–37.
10. Jilka, R.L., Weinstein, R.S., Takahashi, K., Parfitt, A.M., and Manolagas, S.C. 1996. Linkage of decreased bone mass with impaired osteoblastogenesis in a murine model of accelerated senescence. *J. Clin. Invest.* 97:1732–1740.
11. Ducy, P., et al. 2000. Leptin inhibits bone formation through a hypothalamic relay: a central control of bone mass. *Cell.* 100:197–207.
12. Sabatakos, G., et al. 2000. Overexpression of DeltaFosB transcription factor(s) increases bone formation and inhibits adipogenesis. *Nat. Med.* 6:985–990.
13. Takeda, S., et al. 2002. Leptin regulates bone formation via the sympathetic nervous system. *Cell.* 111:305–317.
14. Takeuchi, Y., et al. 2002. Interleukin-11 as a stimulatory factor for bone formation prevents bone loss with advancing age in mice. *J. Biol. Chem.* 277:49011–49018.
15. Kodama, Y., et al. 1998. Reduced expression of interleukin-11 in bone marrow stromal cells of senescence-accelerated mice (SAMP6): relationship to osteopenia with enhanced adipogenesis. *J. Bone Miner. Res.* 13:1370–1377.
16. Rosen, E.D., Walkey, C.J., Puigserver, P., and Spiegelman, B.M. 2000. Transcriptional regulation of adipogenesis. *Genes Dev.* 14:1293–1307.
17. Rosen, E.D., and Spiegelman, B.M. 2001. PPARγ: a nuclear regulator of metabolism, differentiation, and cell growth. *J. Biol. Chem.* 12:37731–37734.
18. Kersten, S., Desvergne, B., and Wahli, W. 2000. Roles of PPARs in health and disease. *Nature.* 405:421–424.
19. Mangelsdorf, D.J., and Evans, R.M. 1995. The RXR heterodimers and orphan receptors. *Cell.* 83:841–850.
20. Tontonoz, P., Hu, E., and Spiegelman, B.M. 1994. Stimulation of adipogenesis in fibroblasts by PPAR γ 2, a lipid-activated transcription factor. *Cell.* 79:1147–1156.
21. Barak, Y., et al. 1999. PPAR γ is required for placental, cardiac, and adipose tissue development. *Mol. Cell.* 4:585–595.
22. Kubota, N., et al. 1999. PPAR γ mediates high-fat diet-induced adipocyte hypertrophy and insulin resistance. *Mol. Cell.* 4:597–609.
23. Rosen, E.D., et al. 1999. PPAR γ is required for the differentiation of adipose tissue in vivo and in vitro. *Mol. Cell.* 4:611–617.
24. Kadowaki, T. 2000. Insights into insulin resistance and type 2 diabetes from knockout mouse models. *J. Clin. Invest.* 106:459–465.
25. Bradley, A. 1987. Production and analysis of chimaeric mice. In *Teratocarcinomas and embryonic stem cells.* E.J. Robertson, editor. IRL Press. Oxford, United Kingdom. 113–151.
26. Keller, G.M. 1995. In vitro differentiation of embryonic stem cells. *Curr. Opin. Cell Biol.* 7:862–869.
27. Akune, T., et al. 2002. Insulin receptor substrate-2 maintains predominance of anabolic function over catabolic function of osteoblasts. *J. Cell Biol.* 159:147–156.
28. Kobayashi, K., et al. 2000. Tumor necrosis factor α stimulates osteoclast differentiation by a mechanism independent of the ODF/RANKL-RANK interaction. *J. Exp. Med.* 191:275–286.
29. Yamauchi, T., et al. 2001. The mechanisms by which both heterozygous peroxisome proliferator-activated receptor γ (PPARγ) deficiency and PPARgamma agonist improve insulin resistance. *J. Biol. Chem.* 276:41245–41254.
30. Thomas, D.M., Hards, D.K., Rogers, S.D., Ng, K.W., and Best, J.D. 1997. Insulin and bone, clinical and scientific view. *Endocrinology and Metabolism.* 4:5–17.
31. Takeda, S., and Karsenty, G. 2001. Central control of bone formation. *J. Bone Miner. Metab.* 19:195–198.
32. Tanaka, T., Yoshida, N., Kishimoto, T., and Akira, S. 1997. Defective adipocyte differentiation in mice lacking the C/EBPβ and/or C/EBPδ gene. *EMBO J.* 16:7432–7443.
33. Wu, Z., et al. 1999. Cross-regulation of C/EBP α and PPAR γ controls the transcriptional pathway of adipogenesis and insulin sensitivity. *Mol. Cell.* 3:151–158.
34. Karsenty, G. 2001. Minireview: transcriptional control of osteoblast differentiation. *Endocrinology.* 142:2731–2733.
35. Nakashima, K., et al. 2002. The novel zinc finger-containing transcription factor osterix is required for osteoblast differentiation and bone formation. *Cell.* 108:17–29.
36. Patel, M.S., and Karsenty, G. 2002. Regulation of bone formation and vision by LRP5. *N. Engl. J. Med.* 346:1572–1574.
37. Suda, T., et al. 1999. Modulation of osteoclast differentiation and function by the new members of the tumor necrosis factor receptor and ligand families. *Endocr. Rev.* 20:345–357.
38. Lecka-Czernik, B., et al. 1999. Inhibition of Osf2/Cbfa1 expression and terminal osteoblast differentiation by PPARγ2. *J. Cell. Biochem.* 74:357–371.
39. Ricote, M., Li, A.C., Willson, T.M., Kelly, C.J., and Glass, C.K. 1998. The peroxisome proliferator-activated receptor-γ is a negative regulator of macrophage activation. *Nature.* 391:79–82.
40. Tolon, R.M., Castillo, A.I., and Aranda, A. 1998. Activation of the prolactin gene by peroxisome proliferator-activated receptor-α appears to be DNA binding-independent. *J. Biol. Chem.* 273:26652–26661.
41. Benson, S., Wu, J., Padmanabhan, S., Kurtz, T.W., and Pershadsingh, H.A. 2000. Peroxisome proliferator-activated receptor (PPAR)-γ expression in human vascular smooth muscle cells: inhibition of growth, migration, and c-fos expression by the peroxisome proliferator-activated receptor (PPAR)-γ activator troglitazone. *Am. J. Hypertens.* 13:74–82.
42. Alliston, T., Choy, L., Ducy, P., Karsenty, G., and

Derynck, R. 2001. TGF-β-induced repression of CBFA1 by Smad3 decreases cbfa1 and osteocalcin expression and inhibits osteoblast differentiation. *EMBO J.* 20:2254–2272.
43. Borton, A.J., Frederick, J.P., Datto, M.B., Wang, X.F., and Weinstein, R.S. 2001. The loss of Smad3 results in a lower rate of bone formation and osteopenia through dysregulation of osteoblast differentiation and apoptosis. *J. Bone Miner. Res.* 16:1754–1764.
44. Fu, M., et al. 2001. Peroxisome proliferator-activated receptor γ inhibits transforming growth factor beta-induced connective tissue growth factor expression in human aortic smooth muscle cells by interfering with Smad3. *J. Biol. Chem.* 276:45888–45894.
45. Ross, S.E., et al. 2000. Inhibition of adipogenesis by Wnt signaling. *Science.* 289:950–953.
46. Bennett, C.N., et al. 2002. Regulation of Wnt signaling during adipogenesis. *J. Biol. Chem.* 277:30998–31004.
47. Bain, G., Muller, T., Wang, X., and Papkoff, J. 2003. Activated β-catenin induces osteoblast differentiation of C3H10T1/2 cells and participates in BMP2 mediated signal transduction. *Biochem. Biophys. Res. Commun.* 301:84–91.
48. Smith, E., Coetzee, G.A., and Frenkel, B. 2002. Glucocorticoids inhibit cell cycle progression in differentiating osteoblasts via glycogen synthase kinase-3β. *J. Biol. Chem.* 277:18191–18197.
49. Garcia, T., et al. 2002. Behavior of osteoblast, adipocyte, and myoblast markers in genome-wide expression analysis of mouse calvaria primary osteoblasts in vitro. *Bone.* 31:205–211.
50. Krakauer, J.C., McKenna, M.J., Rao, D.S., and Whitehouse, F.W. 1997. Bone mineral density in diabetes. *Diabetes Care.* 20:1339–1340.
51. Piepkorn, B., et al. 1997. Bone mineral density and bone metabolism in diabetes mellitus. *Horm. Metab. Res.* 29:584–591.
52. Ogata, N., et al. 2000. Insulin receptor substrate-1 in osteoblast is indispensable for maintaining bone turnover. *J. Clin. Invest.* 105:935–943.
53. Elmquist, J.K., Elias, C.F., and Saper, C.B. 1999. From lesions to leptin: hypothalamic control of food intake and body weight. *Neuron.* 22:221–232.
54. Kallen, C.B., and Lazar, M.A. 1996. Antidiabetic thiazolidinediones inhibit leptin (ob) gene expression in 3T3-L1 adipocytes. *Proc. Natl. Acad. Sci. U. S. A.* 93:5793–5796.
55. Hollenberg, A.N., et al. 1997. Functional antagonism between CCAAT/enhancer binding protein-α and peroxisome proliferator-activated receptor-γ on the leptin promoter. *J. Biol. Chem.* 272:5283–5290.
56. Ogawa, S., et al. 1999. Association of bone mineral density with a polymorphism of the peroxisome proliferator-activated receptor γ gene: PPARγ expression in osteoblasts. *Biochem. Biophys. Res. Commun.* 260:122–126.
57. Nguyen, T.V., Blangero, J., and Eisman, J.A. 2000. Genetic epidemiological approaches to the search for osteoporosis genes. *J. Bone Miner. Res.* 15:392–401.

THE JOURNAL OF BIOLOGICAL CHEMISTRY

Vol. 279, No. 15, Issue of April 9, pp. 15314–15322, 2004
Printed in U.S.A.

Impairment of Bone Healing by Insulin Receptor Substrate-1 Deficiency*

Received for publication, November 16, 2003, and in revised form, January 15, 2004
Published, JBC Papers in Press, January 21, 2004, DOI 10.1074/jbc.M312525200

Takashi Shimoaka‡, Satoru Kamekura‡, Hirotaka Chikuda§, Kazuto Hoshi§, Ung-il Chung§, Toru Akune‡, Zenjiro Maruyama¶, Toshihisa Komori¶, Michihiro Matsumoto‖, Wataru Ogawa‖, Yasuo Terauchi, Takashi Kadowaki**, Kozo Nakamura‡, and Hiroshi Kawaguchi‡ ‡‡**

*From the Departments of ‡Orthopaedic Surgery, §Tissue Engineering, and **Metabolic Diseases, Faculty of Medicine, University of Tokyo, Hongo, Bunkyo, Tokyo 113-8655, ¶Department of Molecular Medicine, Osaka University Medical School, Suita, Osaka 565-0871, and ‖Division of Diabetes, Digestive and Kidney Diseases, Kobe University Graduate School of Medicine, Kobe 650-0017, Japan*

Insulin receptor substrate-1 (IRS-1) is an essential molecule for intracellular signaling of insulin-like growth factor (IGF)-I and insulin, both of which are potent anabolic regulators of bone and cartilage metabolism. To investigate the role of IRS-1 in bone regeneration, fracture was introduced in the tibia, and its healing was compared between wild-type (WT) mice and mice lacking the *IRS-1* gene (*IRS-1*$^{-/-}$ mice). Among 15 *IRS-1*$^{-/-}$ mice, 12 remained in a non-union state even at 10 weeks after the operation, whereas all 15 WT mice showed a rigid bone union at 3 weeks. This impairment was because of the suppression of callus formation with a decrease in chondrocyte proliferation and increases in hypertrophic differentiation and apoptosis. Reintroduction of IRS-1 to the *IRS-1*$^{-/-}$ fractured site using an adenovirus vector significantly restored the callus formation. In the culture of chondrocytes isolated from the mouse growth plate, *IRS-1*$^{-/-}$ chondrocytes showed less mitogenic ability and Akt phosphorylation than WT chondrocytes. An Akt inhibitor decreased the IGF-I-stimulated DNA synthesis of chondrocytes more potently in the WT culture than in the *IRS-1*$^{-/-}$ culture. We therefore conclude that IRS-1 deficiency impairs bone healing at least partly by inhibiting chondrocyte proliferation through the phosphatidylinositol 3-kinase/Akt pathway, and we propose that IRS-1 can be a target molecule for bone regenerative medicine.

In efforts to develop more advanced skeletal regenerative medicine through genetic manipulation, we have been attempting to identify genes implicated in bone and cartilage formation *in vivo*. Healing of bone fracture is composed of complex multistep processes involving a variety of cellular events for bone and cartilage regeneration (1, 2). Under the periosteum adjacent to the fracture gap, undifferentiated mesenchymal cells start differentiation directly to cells of osteoblastic lineage for the membranous ossification, whereas in granulation tissue inside the fracture gap, these mesenchymal cells undergo endochondral bone formation; they differentiate first into chondrocytes to form cartilage which is subsequently replaced by calcified tissues. The size and quality of fracture callus that determine the mechanical property of the fracture site are mostly dependent on the latter process. Because the endochondral bone formation also takes place in embryonic development and in skeletal growth after birth, understanding the molecular mechanism of fracture healing may not only help treat non-union and delayed union of fracture itself but also help advance bone regenerative medicine.

Insulin-like growth factor-I (IGF-I)[1] plays important roles in the anabolic regulation of bone and cartilage metabolism (3). Osteoblasts and chondrocytes produce this growth factor, express its receptor, and respond to it (3, 4). IGF-I appears essential for normal bone development because deletion of IGF-I or its receptor leads to a reduction in bone size at birth (5, 6). Clinically, patients with Laron syndrome caused by IGF-I deficiency exhibit growth retardation and osteoporosis (7). IGF-I is also reported to be expressed during fracture healing and to stimulate it, suggesting a role as an autocrine/paracrine factor potentiating bone regeneration (8, 9). Insulin also plays important roles in the anabolic regulation of bone and cartilage metabolism (10). Although the anabolic effect of insulin on bone may be primarily related to its ability to stimulate osteoblast proliferation, that on cartilage may involve the acceleration of chondrocyte differentiation (11, 12). Patients with insulin deficiency as exemplified by type 1 diabetes mellitus are associated with osteoporosis (13, 14). Diabetes has also been shown to impair fracture healing, which is restored by treatment with insulin in both humans and animals (2, 15, 16).

Both IGF-I and insulin initiate cellular responses by binding to distinct cell-surface receptor tyrosine kinases that regulate a variety of signaling pathways controlling metabolism, growth, and survival. Insulin receptor substrates (IRSs) are essential substrates of the receptor tyrosine kinases, which integrate the pleiotropic effects of IGF-I and insulin on cellular function (17, 18). The mammalian IRS family contains at least four members: ubiquitous IRS-1 and IRS-2, adipose tissue-predominant

* This work was supported by Grants-in-aid for Scientific Research from the Japanese Ministry of Education, Culture, Sports, Science and Technology 11470301 and 12137201, the Uehara Memorial Foundation, and the Takeda Science Foundation. The costs of publication of this article were defrayed in part by the payment of page charges. This article must therefore be hereby marked "*advertisement*" in accordance with 18 U.S.C. Section 1734 solely to indicate this fact.

‡‡ To whom correspondence should be addressed: Dept. of Orthopaedic Surgery, Faculty of Medicine, University of Tokyo, Hongo 7-3-1, Bunkyo, Tokyo 113-8655, Japan. Tel.: 81-3-3815-5411 (ext. 30473 or 33376); Fax: 81-3-3818-4082; E-mail: kawaguchi-ort@h.u-tokyo.ac.jp.

[1] The abbreviations used are: IGF, insulin-like growth factor; IRS, insulin receptor substrate; WT, wild-type; BMC, bone mineral content; HE, hematoxylin-eosin; PCNA, proliferating cell nuclear antigen; PBS, phosphate-buffered saline; TUNEL, terminal transferase dUTP nick end labeling; AxLacZ, adenovirus vector carrying β-galactosidase gene; DMEM, Dulbecco's modified Eagle's medium; PI3K, phosphatidylinositol 3-kinase; MAPK, mitogen-activated protein kinase; ERK, extracellular signal-regulated kinase; FGF, fibroblast growth factor; IGF-IR, insulin-like growth factor-I receptor; SHC, Src homology collagen; X-gal, 5-bromo-4-chloro-3-indolyl-β-D-galactopyranoside; FBS, fetal bovine serum; TdR, [^{3}H]thymidine; PI3K, phosphatidylinositol 3-kinase.

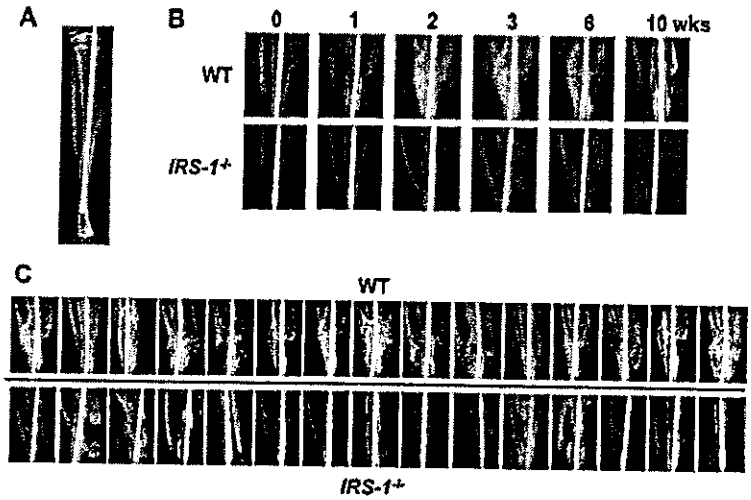

FIG. 1. **X-ray features of bone healing in WT and *IRS-1*$^{-/-}$ mice.** *A*, the fracture model used in this study. After exposing the right tibiae of 8-week-old mice, a transverse osteotomy was performed at the midshaft with a bone saw. The bone marrow cavity was then stabilized with an intramedullary nail. *B*, time course of the fracture healing in representative WT and *IRS-1*$^{-/-}$ mice. *C*, x-ray features of the fracture sites of all WT mice (n = 15) and *IRS-1*$^{-/-}$ mice (n = 15) at 3 weeks after the fracture. Bone union was completed in all 15 WT mice, whereas in *IRS-1*$^{-/-}$ mice, 12 out of 15 showed non-union (the *12 panels at left*).

IRS-3, and IRS-4 which is expressed in the thymus, brain, and kidney. We reported previously that IRS-1 and IRS-2 are expressed in bone (19, 20). Our further studies on bone metabolism of mice lacking the *IRS-1* gene (*IRS-1*$^{-/-}$ mice) or the *IRS-2* gene (*IRS-2*$^{-/-}$ mice) revealed that IRS-1 is important for maintaining bone turnover (19), whereas IRS-2 is important for maintaining predominance of anabolic function over catabolic function of osteoblasts (20). Regarding the role of these molecules on bone growth, IRS-1, but not IRS-2, seems to play an important role in the growth plate function, because *IRS-1*$^{-/-}$ mice were about 20–30% shorter in limbs and trunk, whereas *IRS-2*$^{-/-}$ mice were normal in size as compared with wild-type (WT) littermates (19–22). These data raise an interesting possibility that IRS-1 may be essential for endochondral ossification. To assess this possibility, the present study investigated the role of IRS-1 in bone healing and its mechanism by an *in vivo* fracture model and an *in vitro* culture system.

EXPERIMENTAL PROCEDURES

Animals—Mice in a C57BL6/CBA hybrid background were generated and maintained as reported previously (21). WT and *IRS-1*$^{-/-}$ male littermates generated from the intercross between heterozygous *IRS-1*$^{+/-}$ mice were compared. All experiments were performed according to the protocol approved by the Animal Care and Use Committee of the University of Tokyo.

Fracture Model—Twenty five male mice at 8 weeks of age were used in each group. Under general anesthesia with pentobarbiturate (0.5 mg/10 g body weight, Sigma), the bilateral hind limbs were shaved and sterilized. A 15-mm incision was made longitudinally over the right leg, and a blunt dissection of the muscle was made to expose the tibia. The middle point of the tibia was marked with a surgical marker, and a transverse osteotomy was performed using a bone saw (Volvere GX, NSK Nakanishi Inc., Tochigi, Japan). The fracture was repositioned, and then the full-length of the bone marrow cavity was internally stabilized with an intramedullary nail using the inner pin of a spinal needle of 22- or 23-gauge diameter depending on the size of the cavity. After irrigation with saline, the skin was sutured. The left tibia (unfractured side) was sham-operated and an intramedullary nail of the same size as the control was inserted. No external fixation was used, and the animals were allowed unrestricted activity as well as diet and water *ad libitum*. For histological analyses, animals were killed at 1 (n = 4/group), 3 (n = 3/group), and 6 weeks (n = 3/group) after the operation by diethyl ether, and bilateral tibiae were excised. After extracting the intramedullary nail gently so as not to injure the fracture site, the soft tissue surrounding the tibiae, except for the soft callus around the fracture site, was removed.

Radiological Analysis—X-ray pictures of the right tibiae of WT and *IRS-1*$^{-/-}$ mice (n = 15 each) were taken at 0 (immediately after the operation), 1–3, 6, and 10 weeks after the operation under general anesthesia using a soft x-ray apparatus (CMB-2; Softex Co., Tokyo, Japan). To determine whether there was bone union, bony bridging on radiographs was evaluated by individuals who were blinded with regard to the genotype of mice.

Measurement of Callus Area and Bone Mineral Content (BMC)—Area and BMC of the entire bilateral tibia were measured by a single energy x-ray absorptiometry utilizing a bone mineral analyzer for small animals (PIXIMUS, Lunar Co., Ltd., WI) at 0 (immediately after the operation), 1–4, and 6 weeks after the operation. A preliminary experiment revealed that the intramedullary nail did not affect the BMC value. The gain of area and the % gain of BMC during observation periods as compared with those at time 0 were calculated for both fractured and unfractured sides, and the differences were compared between WT and *IRS-1*$^{-/-}$.

Histological Analysis—Specimens of the harvested tibiae were fixed with 4% paraformaldehyde in 0.1 mol/liter phosphate buffer, pH 7.4, at 4 °C overnight. After decalcification with 4.13% EDTA at 4 °C for 14 days, the tibiae were dehydrated with an increasing concentration of ethanol, embedded in paraffin, and cut into 4-μm-thick sections. The sections were stained with hematoxylin-eosin (HE) or toluidine blue.

Immunohistochemistry—Immunohistochemical localizations of IRS-1, IRS-2, type X collagen, and proliferating cell nuclear antigen (PCNA) were examined in 4-μm dewaxed paraffin sections. After dehydration, the sections were treated with 0.3% hydrogen peroxide in phosphate-buffered saline (PBS) for 30 min at room temperature. After blocking by PBS containing 1% bovine serum albumin (Sigma) for 1 h at room temperature, the sections were incubated in polyclonal rabbit antibody against IRS-1, IRS-2, or type X collagen (Santa Cruz Biotechnology) or monoclonal mouse antibody against PCNA (PC10, Sigma) (23), at a dilution of 1:100 for 24 h at 4 °C. As negative controls, we used non-immune rabbit IgG and mouse IgG of the same dilution instead of the primary antibodies. Then the sections were rinsed in PBS and incubated with the horseradish peroxidase-conjugated goat antibody against rabbit IgG (Dakopatts, Glostrup, Denmark) for immunohistochemistry of IRS-1, IRS-2, and type X collagen, and with the horseradish peroxidase-conjugated goat antibody against mouse IgG (EY Laboratories, Inc., San Mateo, CA) for that of PCNA, respectively, for 1 h at room temperature. After washing with PBS, the sections were immersed in a diaminobenzidine solution for 10 min at room temperature to visualize immunoreactivity. Terminal transferase dUTP nick-end labeling (TUNEL) staining was performed using an Apoptosis *in Situ* Detection kit (Wako Pure Chemical Co., Ltd., Osaka, Japan) according to the manufacturer's instructions.

Generation of Adenoviruses and Gene Transfer—The recombinant adenovirus vector carrying human *IRS-1* gene engineered to express hemagglutinin tag at its N terminus was constructed using an Adenovirus Expression Vector kit (Takara Shuzo Co., Ltd., Shiga, Japan) following the manufacturer's protocol. The adenovirus vector carrying β-galactosidase gene (AxLacZ) was kindly provided by Dr. I. Saito (University of Tokyo). Two days after the operation, a 1×10^{12} plaque-forming units suspension of AxIRS-1 or AxLacZ was injected into the fracture site of *IRS-1*$^{-/-}$ mice as described previously (24, 25). The same dose of AxLacZ was also injected to WT mice as a positive control. Animals were sacrificed at 1 week (n = 3/group) and 3 weeks (n = 3/group) after the injection. To confirm the infection efficiency, expression of *lacZ* was examined by histochemical staining by X-gal staining

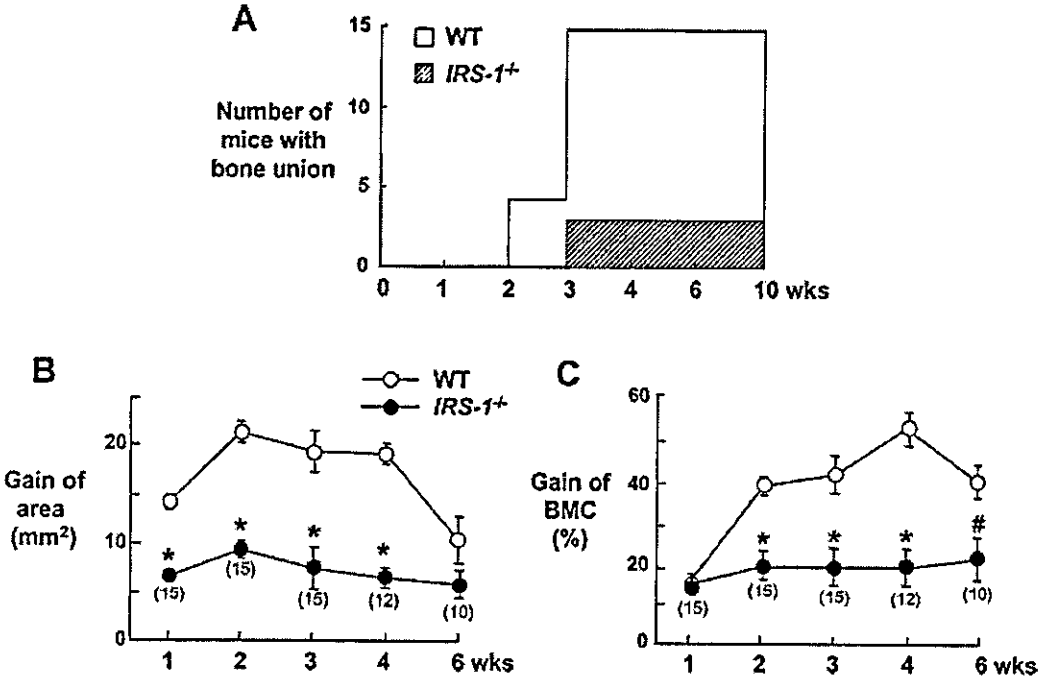

FIG. 2. **Time course of the number of mice with bone union (*A*), the gain of area (*B*), and the % gain of BMC (*C*) at the fracture sites of WT and *IRS-1*$^{-/-}$ mice.** To determine the bone union, the bony bridging at the fracture site on x-rays was judged by individuals blinded with regard to the genotype. The gain of area and the % gain of BMC during observation periods as compared with those at time 0 were calculated for the entire tibiae of fractured and unfractured sides, and the differences were compared between WT and *IRS-1*$^{-/-}$ callus. Because the fracture site became too displaced to measure these parameters correctly at the later stage in *IRS-1*$^{-/-}$ mice, the number of mice was decreased as shown in *parentheses*. Data in *B* and *C* are expressed as the mean (*symbols*) ± S.E. (*error bars*) for 15 WT mice, and the number shown in *parentheses* for *IRS-1*$^{-/-}$ mice. #, $p < 0.05$; *, $p < 0.01$ *versus* WT.

buffer (1 mg/ml X-gal, 5 mM potassium ferrocyanide, and 5 mM potassium ferricyanide) (Wako).

Isolation and Culture of Mouse Growth Plate Chondrocytes—Chondrocytes were isolated from epiphyseal growth plates of WT and *IRS-1*$^{-/-}$ mice at 3.5 weeks of age. Mice were sacrificed, and tibiae were harvested and cleaned of perichondrium in an aseptic manner. Tibiae were pretreated with 0.3% collagenase in serum-free Dulbecco's modified Eagle's medium (DMEM; Sigma) at 37 °C for 30 min to remove residual tissue. By washing the tibiae with PBS, all soft tissues were detached. Growth plates were dissected microscopically by inserting a 26-gauge needle. Subsequently, tibiae were digested with 0.3% collagenase in serum-free DMEM at 37 °C for 5 h, and matrix debris was removed by filtering through a 70-μm cell strainer (BD Biosciences). Chondrocytes were pelleted by centrifugation and washed twice with PBS. Cells were plated in 6-multiwell dishes at a density of 5,000 cells/cm^2 and grown to confluence in DMEM containing 10% FBS and antibiotics in a humidified CO_2 incubator.

X-gal Staining of Chondrocytes Isolated from Transgenic Mice with Type I Collagen Promoter or Type II Collagen Promoter Driving the lacZ Gene—To confirm the purity of chondrocytes isolated by the method above, transgenic mice expressing osteoblast- or chondrocyte-specific marker gene construct (the 2.3-kb fragment of the α1(I) collagen gene promoter or the 1.0-kb fragment of α1(II) collagen promoter and 0.6-kb enhancer) linked to the *Escherichia coli lacZ* gene were used (26, 27). Expression of *lacZ* was examined by histochemical staining with X-gal. Cells were isolated from the growth plates of transgenic mice by the method above and were cultured for 2 days. They were rinsed in PBS twice and fixed with 0.25% glutaraldehyde in PBS on ice for 10 min. After fixed samples were washed in PBS, staining was carried out by the X-gal staining buffer described above at 37 °C overnight.

Western Blot Analysis—To examine the IRS-1 and IRS-2 protein levels, chondrocytes isolated from WT and *IRS-1*$^{-/-}$ growth plates described above were plated in 6-multiwell plates at a density of 10^5 cells/well and incubated in DMEM containing 10% FBS for 24 h. For comparison, we also examined the protein levels in primary osteoblasts that were isolated from neonatal mouse calvariae and cultured in α-minimum Eagle's medium containing 10% FBS as described previously (28). To investigate the signaling pathways through phosphatidylinositol 3-kinase (PI3K)/Akt and mitogen-activated protein kinases (MAPKs), primary chondrocytes were pre-incubated in DMEM containing 10% FBS for 24 h, and treated with IGF-I (10 nM) in the presence and absence of LY294002 (10 μM), PD98059 (10 μM), and SB203580 (10 μM) (all from Calbiochem-Novabiochem) for 30 min. Cells were lysed with TNE buffer (10 mM Tris-HCl, 150 mM NaCl, 1% Nonidet P-40, 1 mM EDTA, 10 mM NaF, 2 mM Na_3VO_4, 1 mM aminoethylbenzenesulfonyl fluoride, and 10 μg/ml aprotinin), and the protein concentration in the cell lysate was measured using a Protein Assay Kit II (Bio-Rad). Equivalent amounts (20 μg) of cell lysates were electrophoresed by 8% SDS-PAGE and transferred to nitrocellulose membrane. After blocking with 5% bovine serum albumin, the membrane was incubated with polyclonal rabbit antibodies against IRS-1 and IRS-2 as described above, Akt, phospho-Akt, extracellular signal-regulated kinase (ERK), phospho-ERK, p38, phospho-p38 MAPK (all from Cell Signaling Technology, Inc. Beverly, MA) and against actin (Sigma). Immunoreactive bands were visualized using the ECL chemiluminescence reaction (Amersham Biosciences) following the manufacturer's instructions. Signals were quantified by densitometry (Bio-Rad).

DNA Synthesis and Proliferation Assays—DNA synthesis and proliferation of isolated chondrocytes were determined by the [^{3}H]thymidine (TdR) uptake and the growth curve, respectively. For the former assay, primary chondrocytes from WT or *IRS-1*$^{-/-}$ mice were inoculated at a density of 5 × 10^4 cells/well in a 24-multiwell plate and cultured to confluency in DMEM, 10% FBS for 2 days. Serum was withheld for 12 h before adding the experimental medium with or without IGF-I (10 nM), LY294002 (1, 3, and 10 μM), PD98059 (1, 3, and 10 μM), and SB203580 (1, 3, and 10 μM). Uptake of [^{3}H]TdR (1 μCi/ml in the medium) added for the final 2 h was measured at 18 h. For the growth curve assay, primary chondrocytes from WT or *IRS-1*$^{-/-}$ mice were inoculated at a density of 10^5 cells/well in 6-multiwell plates in DMEM, 10% FBS and cultured with or without IGF-I (10 nM). The number of cells/well was counted 1, 3, 5, 7, and 9 days after the seeding.

Statistical Analysis—Means of groups were compared by analysis of variance, and significance of differences was determined by post-hoc testing using Bonferroni's method.

RESULTS

Radiological Findings—Fig. 1A shows an x-ray feature of the fracture model that we used in this study. This model was confirmed to show the bone healing process similar to that in

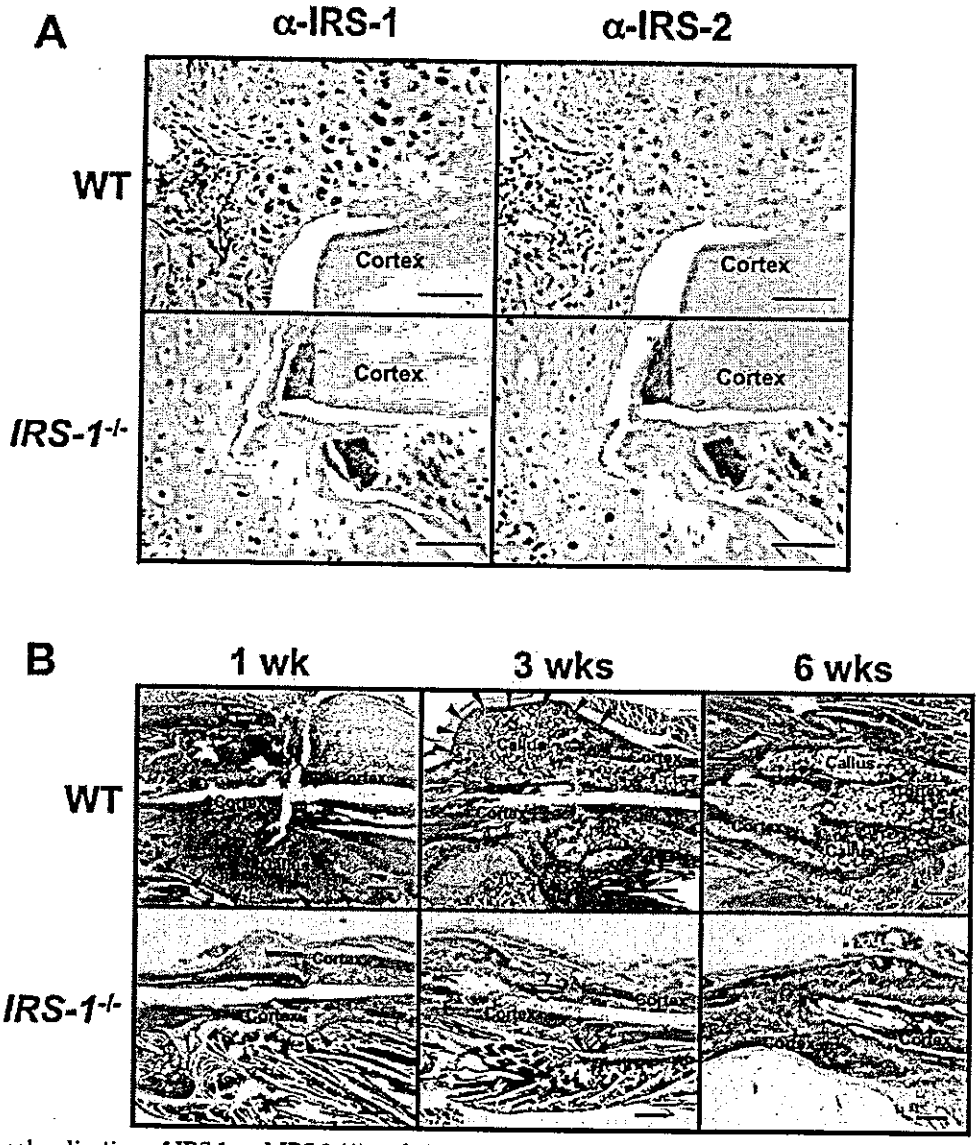

FIG. 3. **Immunolocalization of IRS-1 and IRS-2 (*A*) and time course of histological findings (*B*) at the fracture sites of WT and *IRS-1*$^{-/-}$ mice.** *A*, immunohistochemical stainings with an anti-IRS-1 antibody (*α-IRS-1, left*) and an anti-IRS-2 antibody (*α-IRS-2, right*) were performed on the fracture callus of WT and *IRS-1*$^{-/-}$ mice at 3 weeks. Positive and specific stainings by α-IRS-1 shown in *brown* are seen in fibroblasts and chondrocytes of the WT callus. No immunostaining was observed by the respective non-immune rabbit IgGs as negative controls (data not shown). *Bar*, 100 μm. *B*, 1, 3, and 6 weeks after the fracture, specimens of the harvested tibiae were stained with HE. At 1 week after fracture, the soft callus *outlined* by *arrowheads* is much larger in the WT fracture site than in *IRS-1*$^{-/-}$. At 3 weeks, the WT callus was mineralized as *outlined* by *arrowheads*, which was hardly seen in the *IRS-1*$^{-/-}$ specimen. *Bar*, 1 mm.

humans in a definite temporal sequence by the time course of x-ray examination in WT mice (Fig. 1*B*, *upper panel*). Callus formation could be detected at 1 week, and bony bridging at the fracture site was completed 2 or 3 weeks after the fracture. After the callus size and density reached maximum around 3 weeks, they decreased gradually due to bone remodeling up to 10 weeks. In *IRS-1*$^{-/-}$ mice, however, neither callus formation nor bridging between the fracture stumps was seen at the early stage, and the fracture site became atrophic without bone union at 10 weeks. Fig. 1*C* shows x-ray features of the fracture site of all 15 mice in each of WT and *IRS-1*$^{-/-}$ groups at 3 weeks after fracture. In WT mice, bone union with substantial hard callus formation was observed in all 15 animals. In *IRS-1*$^{-/-}$ mice, however, fracture healing was extremely impaired, and 12 out of 15 mice showed no bone union (the *12 panels at left*). Although bone union was seen in 3 *IRS-1*$^{-/-}$ mice (the *3 panels at right*), the callus looked much smaller and fainter than that of WT mice.

The time course of the number of animals with fracture union determined by bony bridging on x-ray revealed that 4 WT mice achieved bone union at 2 weeks after the operation, and all 15 mice did so at 3 weeks. However, only 3 *IRS-1*$^{-/-}$ mice showed bone union at 3 weeks, but the other 12 animals remained in a non-union state even at 10 weeks (Fig. 2*A*).

Callus Area and BMC—To quantify the callus formation, differences in the gain of area and the % gain of BMC between the fractured and unfractured tibiae were measured by a bone densitometer (Fig. 2, *B* and *C*). Significant differences between WT and *IRS-1*$^{-/-}$ mice were seen from 1 to 4 weeks in the callus area, and from 2 weeks to the end in the BMC. In WT mice, both parameters were increased at the early stage of healing due to the acceleration of the modeling

process and decreased thereafter due to remodeling. In *IRS-1*$^{-/-}$ mice, these parameters remained at low levels throughout the observation period. At the later stage in the *IRS-1*$^{-/-}$ mice, the fracture site became displaced due to non-union, and at 10 weeks more than half the *IRS-1*$^{-/-}$ mice showed severe displacement which was beyond evaluation. To exclude the possibility of other parts of tibiae outside the fracture site affecting BMC, BMC at the bilateral femurs and distal third tibiae was measured at 3 and 6 weeks. Because there were no differences between the fractured and unfractured sides (data not shown), the BMC decrease in *IRS-1*$^{-/-}$ mice was caused by the decrease in that of the callus itself.

Histological Findings—To assess the involvement of IRS-1 and IRS-2 in bone healing, we examined the localizations of these proteins at the fracture site in WT and *IRS-1*$^{-/-}$ mice at 3 weeks after fracture (Fig. 3*A*). Immunohistochemical analysis of WT callus revealed that IRS-1 was localized at various cells including chondrocytes and fibroblasts, although IRS-2 immunoactivity was very faint. In *IRS-1*$^{-/-}$ mice, both IRS-1 and IRS-2 proteins were barely detectable at the fracture site, suggesting that there was no compensatory up-regulation of IRS-2 by IRS-1 deficiency.

Fig. 3*B* shows the temporal comparison of histology between WT and *IRS-1*$^{-/-}$ fracture sites. At 1 week after fracture, tissue reaction was seen in the large areas around the fracture gap in WT mice, whereas in *IRS-1*$^{-/-}$ mice it was markedly decreased, resulting in the reduced size of soft callus. At 3 weeks, mineralized and hard callus due to endochondral ossification was abundantly observed in WT mice, whereas fibrous tissue remained at the fracture gap in *IRS-1*$^{-/-}$ mice. At 6 weeks, bony union after the remodeling was completed in WT mice. However, in *IRS-1*$^{-/-}$ mice, fibrous tissue still remained in the fracture gap, indicating a state of non-union. Thus, the impairment of fracture healing in *IRS-1*$^{-/-}$ mice was seen from the early stage of fracture healing, at which time the required amount of soft callus must be formed.

To learn the cellular and molecular mechanisms of impaired bone healing at the early stage due to IRS-1 deficiency, we performed more detailed histological analyses of the fracture callus at 1 week (Fig. 4). Although the size of soft callus was much smaller in *IRS-1*$^{-/-}$ mice than in WT mice, the chondrocyte differentiation in this small cartilage of *IRS-1*$^{-/-}$ mice was more advanced than that of WT mice as shown by the toluidine blue staining (Fig. 4, *A* and *B*). Type X collagen, a marker for hypertrophic chondrocytes, was much more prevalent in *IRS-1*$^{-/-}$ cartilage than in WT cartilage (Fig. 4, *C* and *D*). We further investigated the proliferation and apoptosis of chondrocytes by PCNA and TUNEL stainings, respectively. PCNA-positive proliferative cells were found massively at the WT callus, although they were faint and scant in the *IRS-1*$^{-/-}$ callus (Fig. 4, *E* and *F*). In contrast, TUNEL-positive apoptotic cells were hardly visible in WT, whereas they were abundant in hypertrophic chondrocytes of *IRS-1*$^{-/-}$ (Fig. 4, *G* and *H*). These findings indicate that the suppression of callus formation in the *IRS-1*$^{-/-}$ fracture site was associated with a decrease in chondrocyte proliferation and increases in hypertrophic differentiation and apoptosis.

Restoration by Reintroduction of IRS-1 in the IRS-1$^{-/-}$ *Fracture*—To confirm that the impairment in fracture healing was due simply to the IRS-1 deficiency in these mice, we injected an adenovirus vector carrying *IRS-1* gene (AxIRS1) or *lacZ* (AxLacZ) to the fracture site 2 days after the fracture. The transgene expression was confirmed by the X-gal staining in and around the AxLacZ-injected fracture sites, which was positively observed intracellularly in various differentiation stages

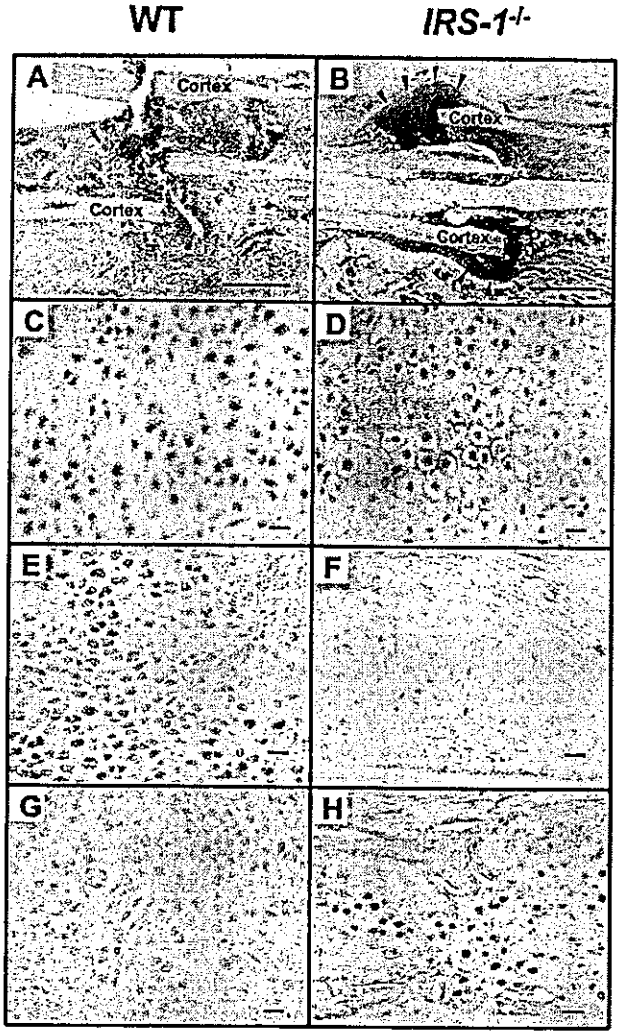

FIG. 4. **Histological and immunohistochemical findings of the soft callus of WT (*A*, *C*, *E*, and *G*) and *IRS-1*$^{-/-}$ mice (*B*, *D*, *F*, and *H*) 1 week after the fracture; toluidine blue (*A* and *B*), type X collagen (*C* and *D*), PCNA (*E* and *F*), and TUNEL (*G* and *H*) stainings.** The 4-μm-thick sections prepared as described for the HE staining were used for the toluidine blue staining. In the WT specimen, the entire fibrous tissue below the fracture site, which is hardly stained with toluidine blue, is the soft callus, whereas in the *IRS-1*$^{-/-}$ specimen, the soft callus *outlined* by *arrowheads* was much smaller but more positively stained (*A* and *B*). Immunohistochemical stainings for type X collagen and TUNEL were examined in 4-μm dewaxed paraffin sections as described under "Experimental Procedures." Both type X collagen-expressing hypertrophic chondrocytes (*C* and *D*) and TUNEL-positive apoptotic cells (*G* and *H*) were more prevalent in the *IRS-1*$^{-/-}$ callus than in WT. On the contrary, PCNA-positive proliferative cells were rarely seen in the *IRS-1*$^{-/-}$ callus (*E* and *F*). No immunostaining was observed by the respective non-immune IgGs as negative controls (data not shown). *Bar*, 1 mm (*A* and *B*) and 10 μm (*C–H*).

of mesenchymal cells (data not shown). AxIRS1 reintroduction to the *IRS-1*$^{-/-}$ fractured site restored the callus area at 1 and 3 weeks, and the callus BMC at 3 weeks after the injection (Fig. 5*A*). Although the restorations did not fully reach the levels of the WT callus injected with AxLacZ, AxIRS1 produced a substantial callus at 1 week (Fig. 5*B*), and all 3 *IRS-1*$^{-/-}$ mice injected with AxIRS-1 showed bony union at 3 weeks, whereas all those injected with AxLacZ remained in a non-union state. It was therefore confirmed that the IRS-1 deficiency *in situ* caused the impaired fracture healing.

Analyses of Cultured Primary Chondrocytes—To clarify fur-